

Thran, M. C., Brune, S., Webster, J. M., Dominey-Howes, D., Harris, D. (2021): Examining the impact of the Great Barrier Reef on tsunami propagation using numerical simulations. - Natural Hazards, 108, 347-388.

<https://doi.org/10.1007/s11069-021-04686-w>

Examining the impact of the Great Barrier Reef on tsunami propagation using numerical simulations

Amanda C. Thran^{1*}, Sascha Brune^{2,3}, Jody M. Webster⁴, Dale Dominey-Howes⁵,

Daniel Harris⁶

¹Water Research Laboratory, School of Civil and Environmental Engineering, University of
New South Wales, Sydney, New South Wales 2052, Australia.

²GFZ German Research Centre for Geosciences, Telegrafenberg, 14473 Potsdam, Germany.

³Institute of Geosciences, University of Potsdam, Potsdam, Germany

⁴Geocoastal Research Group, School of Geosciences, University of Sydney, Sydney, New
South Wales 2050, Australia.

⁵Asia-Pacific Natural Hazards and Disaster Risk Research Group, School of Geosciences,
University of Sydney, Sydney, New South Wales 2050, Australia.

⁶School of Earth and Environmental Sciences, University of Queensland, Brisbane,
Queensland 4072, Australia.

*Corresponding author: m.thran@unsw.edu.au, +61 452 608 228

Author ORCID IDs:

- A. Thran: 0000-0002-0885-3126
- S. Brune: 0000-0003-4985-1810
- J. Webster: 0000-0002-0005-6448
- D. Dominey-Howes: 0000-0003-2677-2837
- D. Harris: 0000-0002-3275-323X

Declarations

26
27

28 **Funding:** A. T. was supported by the University of Sydney DBH Scholarship, and S. B. was
29 supported through the Helmholtz Young Investigators Group CRYSTALS (VH-NG-1132).

30

31 **Conflicts of interest/Competing interests:** The authors have none to declare.

32

33 **Availability of data and material:** The bathymetry of the Great Barrier Reef region can be
34 found here: <http://eatlas.org.au/data/uuid/200aba6b-6fb6-443e-b84b-86b0bbdb53ac>. The
35 Great Barrier Reef Banks shapefile can be obtained here: [https://data.gov.au/dataset/ds-ga-](https://data.gov.au/dataset/ds-ga-c00ab093-f02d-5b03-e044-00144fdd4fa6/details?q=great%20barrier%20reef%20banks)
36 [c00ab093-f02d-5b03-e044-00144fdd4fa6/details?q=great%20barrier%20reef%20banks](https://data.gov.au/dataset/ds-ga-c00ab093-f02d-5b03-e044-00144fdd4fa6/details?q=great%20barrier%20reef%20banks). The
37 global reef dataset can be downloaded here: [www.wri.org/resources/data-sets/reefs-risk-](http://www.wri.org/resources/data-sets/reefs-risk-revisited)
38 [revisited](http://www.wri.org/resources/data-sets/reefs-risk-revisited).

39

40 **Code availability:** The code Geowave can be downloaded here:

41 <http://www.appliedfluids.com/geowave.html>. The codes NHWAVE and FUNWAVE-TVD
42 can be downloaded from GitHub (github.com/JimKirby/NHWAVE;
43 [fengyanshi.github.io/build/html/index.html](https://github.com/fengyanshi/fengyanshi.github.io/build/html/index.html)).

44

Abstract

45 Coral reefs may provide a beneficial first line of defence against tsunami hazards, though this
46 is currently debated. Using a fully nonlinear, Boussinesq propagation model, we examine the
47 buffering capacity of the Great Barrier Reef against tsunamis triggered by several hypothetical
48 sources: a series of far-field, Solomon Islands earthquake sources of various magnitudes (M_w
49 8.0, M_w 8.5, and M_w 9.0), a submarine landslide source that has previously been documented
50 in the offshore geological record (i.e. the Gloria Knolls Slide), and a potential future landslide
51 source (i.e. the Noggin Block). We show that overall, the Great Barrier Reef acts as a large-
52 scale regional buffer due to the roughness of coral cover and the complex bathymetric features
53 (i.e. platforms, shoals, terraces, etc.) that corals construct over thousands of years. However,
54 the buffering effect of coral cover is much stronger for tsunamis that are higher in amplitude.
55 When coral cover is removed, the largest earthquake scenario (M_w 9.0) exhibits up to a 31%
56 increase in offshore wave amplitude and estimated run-up. These metrics increase even more
57 for landslide scenarios, where they tend to double. These discrepancies can be explained by the
58 higher bed particle velocities incited by higher-amplitude waves, which leads to greater
59 frictional dissipation at a seabed covered by coral. At a site-specific level, shoreline orientation
60 relative to the reef platforms also determines the degree of protectiveness against both types of
61 tsunamis, where areas situated behind broad, shallow, coral-covered platforms benefit the
62 most. Additionally, we find that the platforms, rather than gaps in the offshore reef structure,
63 tend to amplify wave trains through wave focussing when coral cover is removed from
64 simulations. Our findings have implications for future tsunami hazards along the northeastern
65 Australian coastline, particularly as the physiological stressors imposed by anthropogenic
66 climate change further exacerbate coral die-off and reductions in ecosystem complexity.
67 Therefore, areas that experience a protective benefit by the Great Barrier Reef's platforms
68 could be disproportionately more vulnerable in the future.

69

70 Keywords:

71 coral reef, tsunami, Great Barrier Reef, submarine landslide, earthquake, numerical

72 simulation

73

Draft manuscript

74 1. Introduction

75

76 Tsunamis threaten low-lying coastal communities around the world. Coral reef ecosystems,
77 many of which are positioned between tsunami source regions and densely-populated
78 shorelines (Figure 1), could provide a broad, cost-effective first line of defence for coastal
79 zones (Ferrario et al. 2014). While field-based studies suggest that coral reefs induce efficient
80 energy attenuation in wind waves due to their structural complexity (Sheppard et al. 2005;
81 Ferrario et al. 2014; Gallop et al. 2014), a lack of consensus endures surrounding their
82 protectiveness against tsunamis.

83

84 Following a similar logic, some post-inundation field surveys (Fernando et al. 2005; McAdoo
85 et al. 2011) and modelling studies (Shao et al. 2019) have concluded that, due to their structural
86 complexity, coral reef ecosystems impart similar drag-induced attenuation of wave energy on
87 tsunamis. Other field-based studies (McAdoo et al. 2009; Fritz et al. 2011; Gelfenbaum et al.
88 2011) and modelling work (Kunkel et al. 2006; Yao et al. 2012; Roger et al. 2014) echo these
89 conclusions, but with caveats. For instance, some authors caution that the buffering effect of
90 the reef depends on where the reef is located relative to a coastal community or built asset
91 (McAdoo et al. 2009; Fritz et al. 2011), and that wider reefs, preferably those with an extensive
92 reef flat, appear to dissipate tsunami energy more effectively than narrower fringing reefs
93 (Kunkel et al. 2006; Gelfenbaum et al. 2011; Yao et al. 2012; Roger et al. 2014). Conversely,
94 others have proposed that coral reefs offer marginal to no protective benefit against tsunamis
95 (Baird et al. 2005; Uslu et al. 2010). Further still, some field-based (Nott 1997; Chatenoux and
96 Peduzzi 2005, 2007; Fritz et al. 2011) and modelling work (Roeber et al. 2010; Gelfenbaum et
97 al. 2011; Yao et al. 2012; Ford et al. 2014) suggest that reefs can actually exacerbate damage
98 along neighbouring coastlines. While there is near-universal consensus that inter-reef passages
99 (or “gaps/openings” between reefs) can amplify tsunami waves, some argue that these

100 amplification effects, along with other effects such as intra-lagoon resonance and increased
101 shoaling/bore formation over shallow reef platforms, undermine any protective benefit that the
102 presence of the reef would otherwise offer (Chatenoux and Peduzzi 2005; Liu et al. 2005;
103 Roeber et al. 2010; Gelfenbaum et al. 2011; McAdoo et al. 2011; Ford et al. 2014; Roger et al.
104 2014). Despite the wide variety of methods and case studies employed to investigate this topic,
105 the impact of coral reef ecosystems on tsunami propagation remains unclear.

106

107 Ongoing threats to the health and longevity of coral reefs under a changing climate (De'ath et
108 al. 2012; Hughes et al. 2018) heighten these uncertainties. Decades-long field-based studies
109 reveal declines in both coral cover and ecosystem structural complexity as critical reef-building
110 species disappear from coral communities, leading to a progressive “flattening” of reefs
111 (Alvarez-Filip et al. 2009; Bozec et al. 2015; Spalding and Brown 2015). It has been proposed
112 that this decline in coral cover will reduce the protectiveness of coral reefs against other
113 common coastal hazards, such as flooding, wind-wave exposure (both under fair weather and
114 stormy conditions), and rising sea levels (Quataert et al. 2015; Harris et al. 2018; Storlazzi et
115 al. 2018). The literature surrounding the impact of anthropogenically-mediated coral decline
116 on tsunami hazards is less conclusive. However, some evidence from post-tsunami field
117 surveys suggests that direct coral removal by means of mining and poaching intensifies tsunami
118 wave heights and inundation extents at a local level (Fernando et al. 2005). In light of recent
119 coral reef decline, and in the wake of recent significant tsunami events (e.g., the 2004 Indian
120 Ocean tsunami, the 2009 South Pacific tsunamis, and the 2011 Tōhoku tsunami), a concerted
121 effort has emerged to more rigorously assess both the present and future coastal buffering role
122 of coral reef ecosystems against tsunamis (Chatenoux and Peduzzi 2007; Ferrario et al. 2014;
123 Spalding et al. 2014), and this study is a contribution to that effort.

124

125 The Great Barrier Reef (GBR), the world's largest coral reef system, is an iconic feature of
126 Australia's coastal landscape. Despite Australia's proximity to the seismically active source-
127 regions (Dominey-Howes 2007; Davies and Griffin 2018), the manner in which tsunami
128 behaviour is regulated by the GBR, which partitions Australia's coastline from these
129 convergent margins, is not well understood (Webster et al. 2016). Additionally, the discovery
130 of large (volume > 30 km³) landslide scars and slumps on the nearby continental slope (Puga-
131 Bernabéu et al. 2016, 2019) warrants an investigation into the GBR's ability to protect against
132 landslide-generated tsunamis. Though believed to occur less frequently than their coseismic
133 counterparts, landslide-generated tsunamis such as the 1998 Sissano, Papua New Guinea event
134 (Synolakis et al. 2002) can occur suddenly within close proximity to the shoreline, causing
135 significant localized damage and limiting opportunities for warning and swift response. This,
136 along with the existence of possible paleo-tsunami deposits along the adjacent coastline (Nott
137 1997), underscores an urgency to quantify the GBR's widely-speculated role as a regional
138 buffer from these hazards (Baba et al. 2008; Puga-Bernabéu et al. 2013a; Wei et al. 2015; Xing
139 et al. 2015; Webster et al. 2016). However, like most coral reefs worldwide, the GBR has not
140 escaped the consequences of anthropogenic climate change (De'ath et al. 2012; Hughes et al.
141 2018), and therefore, the buffering capacity of the GBR remains uncertain.

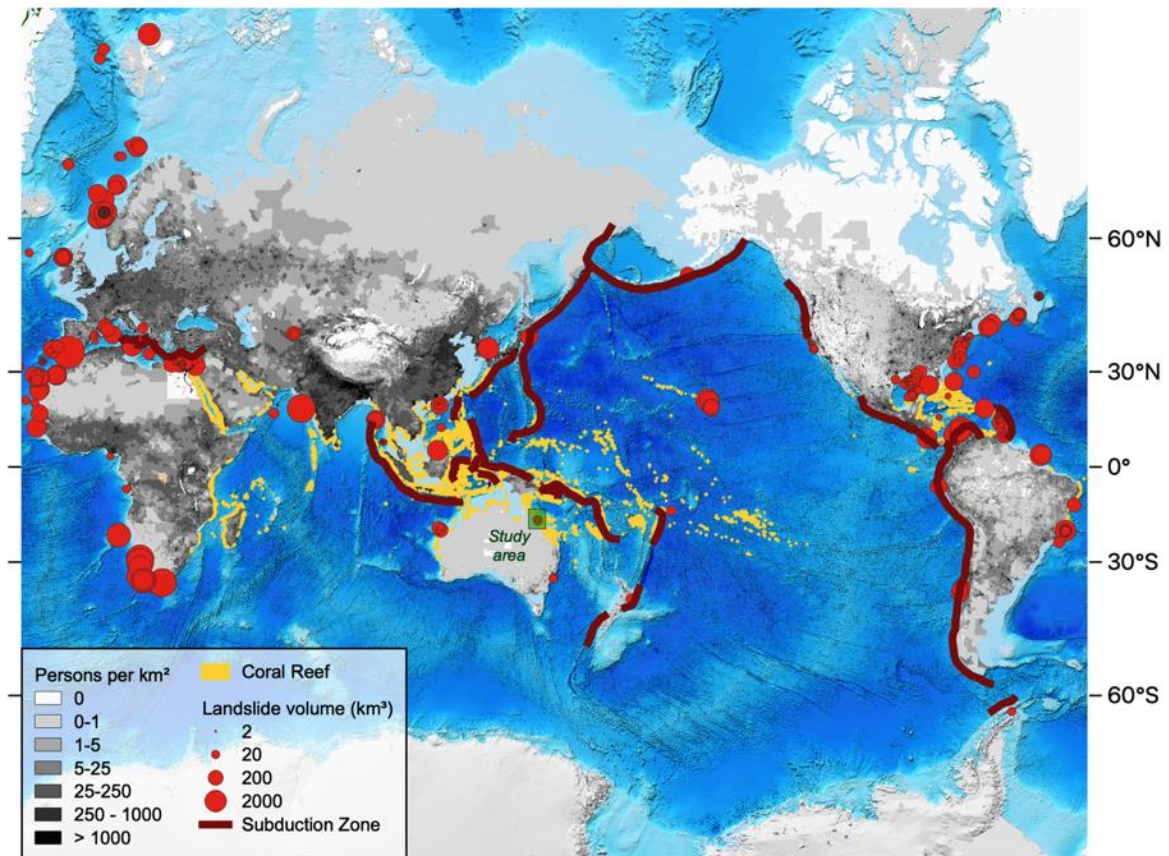
142

143 Thus far, a large portion of the debate surrounding coral reef protectiveness against tsunamis
144 is based on findings from post-tsunami field surveys and anecdotal eye-witness accounts
145 (Baird et al. 2005; Fernando et al. 2005; Liu et al. 2005). However, the degree of a coral reef's
146 influence cannot be quantified solely from these field-based techniques. As many others have
147 highlighted (Chatenoux and Peduzzi 2005; Kunkel et al. 2006; McAdoo et al. 2009; Uslu et al.
148 2010; Roger et al. 2014; Dilmen et al. 2018), several confounding factors can influence tsunami
149 run-up, such as the extent of coral cover, the nature and proximity of the tsunami triggering

150 source, and site-specific variability in coastal bathymetry and topography. Therefore, following
151 a tsunami event, it is difficult to retrospectively ascertain the impact of coral reefs in isolation
152 from these other site-specific factors. Numerical simulations can provide additional insights
153 into tsunami behaviour (e.g., Kunkel et al. 2006), where experiments can be designed to
154 systematically test the impact of coral cover and reef platform bathymetry on tsunami
155 attenuation while keeping all other parameters, initial conditions, and boundary conditions
156 constant (e.g., Kunkel et al. 2006). Previous studies have aimed to assess the overall impact of
157 the GBR on tsunami propagation using numerical simulations (Baba et al. 2008; Wei et al.
158 2015; Xing et al. 2015; Webster et al. 2016). However, they do not account for smaller-scale
159 structural complexity introduced by coral cover on reef platforms, and they only consider one
160 type of tsunami source at a time.

161

Draft manuscript



162

163 **Figure 1.** Global distribution of shallow-water coral reefs (Burke et al. 2011) and their proximity to tsunamigenic
 164 sources, including large submarine landslides or landslide complexes (>1 km³; see Online Resource 1 for table of
 165 landslide events) and submarine convergent plate boundaries that constitute source-zones of major tsunamigenic
 166 earthquakes. Landslides are plotted as red circles sized proportionally to the natural log of a given landslide's
 167 volume. This compilation is based on several reviews (Hampton et al. 1996; Elverhøi et al. 2002; Owen et al.
 168 2007; Lee 2009; Urlaub et al. 2013; Harbitz et al. 2014; Papadopoulos et al. 2014; Moscardelli and Wood 2016),
 169 where landslides with estimated volumes of 1 km³ were excluded. All original references documenting each of
 170 the plotted slides are provided in the reference list of this study. Landmasses are overlaid with gridded UN-
 171 adjusted population density for 2020 (CIESIN 2018), with ETOPO1 as the base map (Amante and Eakins 2009).

172

173 Using numerical modelling, we evaluate the GBR's ability to shield the northeastern Australian
 174 coastline from a range of hypothetical, though plausible tsunami sources. Firstly, we consider
 175 a Solomon Islands earthquake source over various magnitudes (M_w 8.0, M_w 8.5, and M_w 9.0).
 176 Additionally, we consider two near-field landslide tsunami sources: 1) the largest documented
 177 submarine landslide event on the GBR margin (i.e. the Gloria Knolls landslide complex; Puga-
 178 Bernabéu et al. 2016), and 2) a potential collapse of a feature on the upper continental slope
 179 known as the Noggin Block (Puga-Bernabéu et al. 2013a).

180

181 In the first of a series of tsunami propagation model runs, for each tsunami source, we
182 numerically simulate the tsunamis assuming healthy coral cover conditions (i.e. “coral-covered
183 platforms” scenarios), where reef platforms are prescribed high roughness to reflect their
184 structural complexity (Nelson 1996). Then, we simulate the tsunamis with smoothed reef
185 platforms (i.e. “smooth platforms” scenarios), where we isolate the impact of live coral cover
186 on wave attenuation (Sheppard et al. 2005). Following the methods of Baba et al. (2008), we
187 further sequester the region’s bathymetric complexity by completely excising the reef
188 platforms from the shelf and simulating tsunami propagation with altered bathymetry (i.e. “no
189 reef platforms” scenarios), allowing us to assess the platform-scale buffering capacity of the
190 entire reef structure. We further test the impact of tidal phase on the buffering capacity of the
191 GBR. We then draw upon these findings to consider the broader implications regarding present
192 and future coral reef defence to densely inhabited, low-lying coastal areas.

193

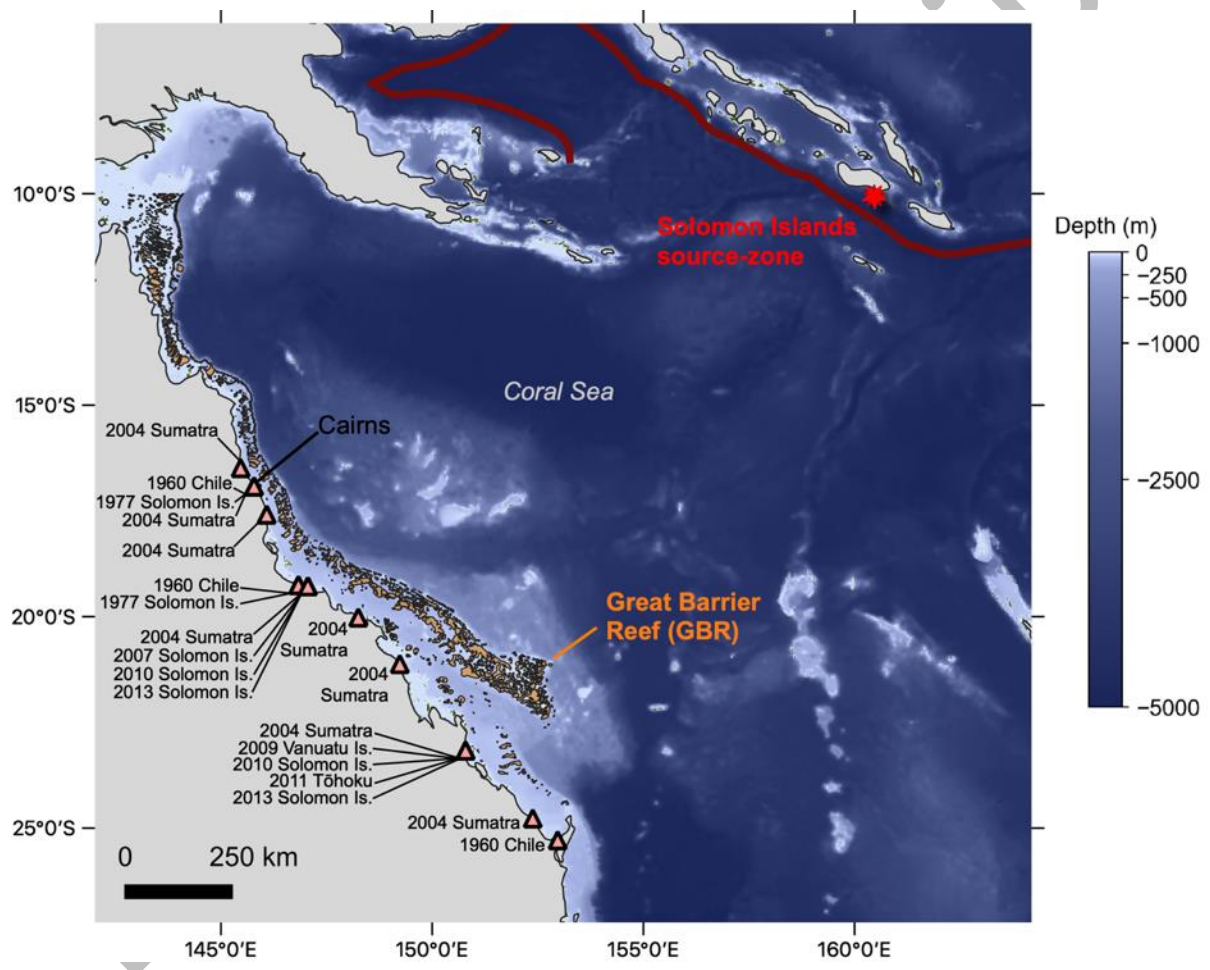
194 2. Study area

195 2.1. Regional Setting

196

197 The central northeastern Australian margin is a passive margin characterised by a relatively
198 broad (~60 km) continental shelf (Figure 2). The spring tidal range varies from north to south,
199 but the region is generally meso- to macro-tidal (Andrews and Bode 1988). Several
200 environmental factors favour coral reef growth on the mid- to outer-continental shelf, including
201 the region’s tropical climate, shallow seas, far proximity from terrestrial run-off, and nutrient-
202 poor oceanographic conditions. Over hundreds of thousands of years of eustatic sea level
203 fluctuations, these coral reef ecosystems have constructed large (up to ~300 km²) submerged
204 and semi-submerged carbonate platforms, pinnacles, and terraces, which comprise the offshore

205 reef structure (Hopley et al. 2007; Hinestrosa et al. 2016). This reef structure, which underlies
 206 the modern generation of living coral cover, extends roughly 2,300 km along the mid- to outer
 207 shelf (Hopley et al. 2007). On the central margin, broad, arcuate patch reef platforms are
 208 separated by relatively wide (up to ~10 km) inter-reef passages, or “gaps” (Figure 3). While
 209 these passages are wide enough to allow some wind waves to propagate through to the inner
 210 shelf, much of the energy transferred by wind waves is attenuated atop the reef platforms
 211 (Young 1989; Gallop et al. 2014).



212

213 **Figure 2.** Regional view of the Solomon Islands source-zone, the Coral Sea, and the northeastern Australian
 214 margin, which includes the GBR (orange). Also plotted are the locations along the Australian coastline where
 215 historical tsunamis that exceeded maximum water heights of 10 cm have been observed using tide gauges
 216 (triangles; NGDC/WDS 2020). The red line indicates the subduction zones that traverse the Solomon Islands
 217 source zone.

218

219

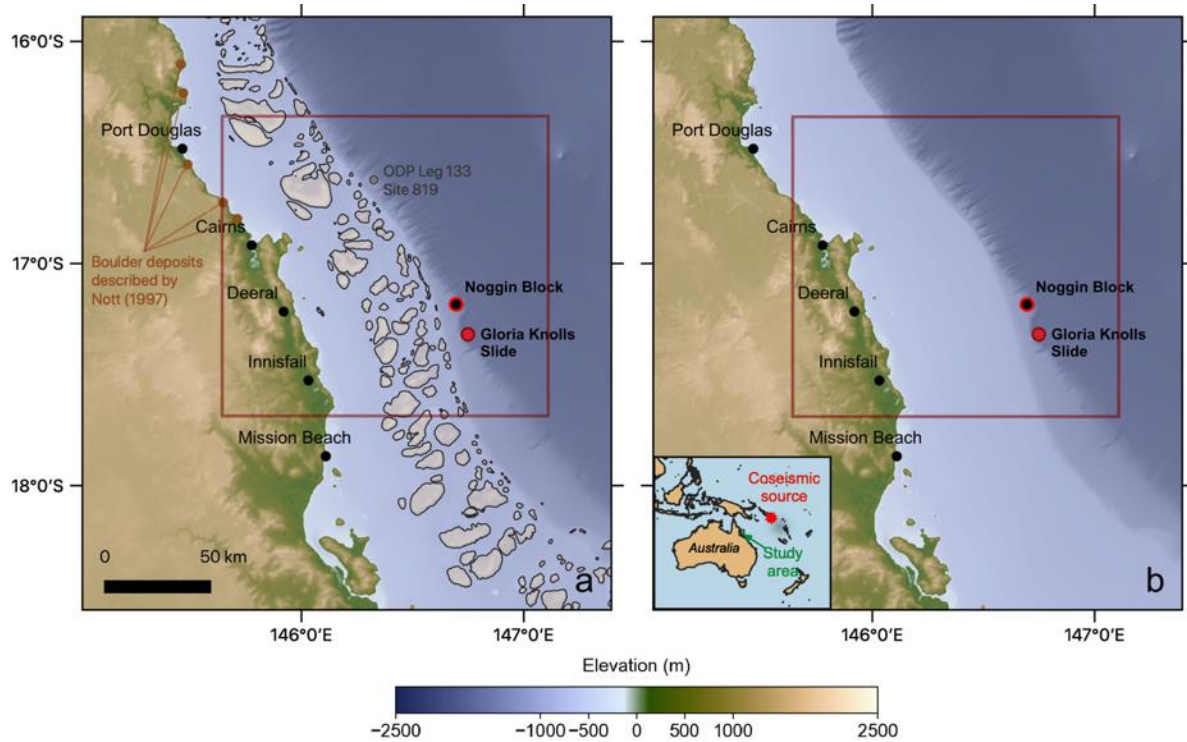
220

221 2.2. Historical and pre-historic tsunami record

222

223 Historically, northeastern Australia has been affected by tsunamis originating from multiple
224 regions contained within the Pacific Ring of Fire (e.g. Chile, Tonga, and more recently,
225 Sumatra and Japan; see Figure 2). Notably, a large proportion of these historical tsunami events
226 were triggered within subduction zones in the Solomon Islands region, which lies to the
227 northeast of Australia across the Coral Sea (Dominey-Howes 2007; Australian Bureau of
228 Meteorology 2020; NGDC/WDS 2020). A nationwide, probabilistic tsunami hazard
229 assessment revealed that the Solomon Islands source-zone poses the greatest hazard to the
230 northeastern Australian town of Cairns and the surrounding area (Davies and Griffin 2018).
231 Therefore, the Solomon Islands source-zone was selected to simulate a range of hypothetical
232 earthquake-generated tsunami events for this study. In contrast, the prehistoric tsunami record
233 in northeastern Australia is much more sparse (Dominey-Howes 2007). Nonetheless, previous
234 work has described boulder deposits that were speculated to have been emplaced by tsunami
235 waves (Nott 1997; Figure 3).

236



237

238 **Figure 3.** a) Bathymetry used in the “coral-covered platforms” and “smooth platforms” simulations. b)
 239 Bathymetry used in the “no reef platforms” simulations. Also shown are the Gloria Knolls Slide, Noggin Block,
 240 ODP Leg 133 Site 819, the locations of the boulder deposits described by Nott (1997) and the location of the
 241 hypothetical Solomon Islands coseismic sources.

242

243 2.3. Submarine landslides and areas of potential future collapse

244

245 Since the collection of high-resolution multibeam bathymetry in 2007 (Webster et al. 2008), a
 246 wide variety of submarine landslides have been described on the shelf-edge, upper, mid, and
 247 lower-slope (Puga-Bernabéu et al. 2016, 2019; Webster et al. 2016). These slides exhibit a
 248 range of different sizes and morphologies (e.g. rotational slumps, translational slides, shovel
 249 slides, carbonate terrace collapses, etc.). While they are distributed along the entirety of the
 250 margin, landslides are more commonly found on the north and central sections of the margin,
 251 where the continental slope gradient is moderate to high (4-10°, Puga-Bernabéu et al. 2011,
 252 2013b).

253

254 The present study focuses on two notable features on the central GBR margin. The first is the
255 Gloria Knolls landslide complex (Puga-Bernabéu et al. 2016), which is the largest among the
256 documented submarine landslide cases on the northeastern Australian margin (total estimated
257 volume $\approx 32 \text{ km}^3$). The entire complex is believed to have failed in multiple phases, with the
258 estimated age of the first event pre-dating 300 ka (Puga-Bernabéu et al. 2016). Debris from the
259 slide is visible in both sub-bottom profiles and in bathymetry, where the debris field extends
260 $\sim 20 \text{ km}$ from the slide scarp. Roughly 8 km northwest of the Gloria Knolls slide complex lies
261 the Noggin Block, a 4.9 x 3.5 km upper-slope feature that was previously identified as a
262 potential area of future collapse (Puga-Bernabéu et al. 2013a). Pockmarks and adjacent
263 landslide scars have also been described around the block (Puga-Bernabéu et al. 2013a). Slope
264 stability modelling indicates that while the block is presently stable, seismic loading could
265 potentially trigger a future failure (Puga-Bernabéu et al. 2013a).

266

267 We should note that it lies beyond the scope of this work to include a detailed catalogue, and
268 thus a detailed hazard assessment, of landslide tsunami risk on this margin. A complete
269 catalogue of all submarine landslides on the GBR margin is currently the subject of future work
270 (Puga-Bernabéu et al., in prep).

271

272 3. Methods

273

274 3.1. Tsunami generation

275 3.1.1. Earthquake sources

276 To simulate tsunami generation by an earthquake source, the code Geowave (Watts et al. 2003)
277 was used to produce the initial ocean free surface deformation for the hypothetical M_w 8.0, 8.5,
278 and 9.0 coseismic events in the Solomon Islands source-zone. Tsunami generation is

279 specifically handled in the TOPICS module of Geowave (Watts et al. 2003). The code
 280 incorporates the widely-implemented Okada elastic half-space formulation, which relates
 281 earthquake geometric source parameters (e.g. fault width, length, strike, dip, etc.) to the initial
 282 free surface deformation (Okada 1985). The Okada method has been shown to adequately
 283 reproduce free surface deformation for coseismic events exhibiting an abrupt, mostly vertical
 284 slip of the seafloor (Kowalik et al. 2005; Fujii et al. 2011) and specifically for past events that
 285 originated in the Solomon Islands (Baba et al. 2008). Source parameters were selected from
 286 the Enhanced Tsunami Scenario Database T2 (Greenslade et al., 2009; see Table 1), a suite of
 287 earthquake tsunami scenarios developed by the Joint Australian Tsunami Warning Centre and
 288 the Centre for Australian Weather and Climate Research. For simplicity, magnitude was altered
 289 by modifying the maximum fault slip parameter (see Table 1).

290 **Table 1.** List of input parameters used for tsunami wave generation models. Cases include the hypothetical Solomon Islands
 291 earthquake source (M_w 8.0, 8.5, and 9.0 scenarios), the Gloria Knolls Slide, and the Noggin Block potential landslide.
 292 Landslide volumes were calculated using the formulas of Enet & Grilli (2007), which are incorporated into NHWAVE.

Hypothetical Solomon Islands Earthquake Cases				Landslide Cases		
				Gloria Knolls Slide (worst case scenario)	Noggin Block Potential Landslide	
M_w	8.0	8.5	9.0	Latitude	17°19'21.9"S	18°46'48"S
Maximum slip distance (m)	0.8	4.4	24.7	Longitude	146°45'07.4"E	148°12'01"E
Centroid latitude	9°50'13.2"S			Length b (m)	3947	4900
Centroid longitude	160°37'55.2"E			Width w (m)	19200	3500
Strike (°)	300			Maximum thickness T (m)	288	150
Dip (°)	30			Slide volume (km ³)	6.51	0.767
Slip rake (°)	90			Initial submergence depth d (m)	420	600
Fault length (km)	400			Mean slope θ (°)	18.6	5.00
Fault centroid depth (km)	10			Slide density (kg/m ³)	2000	2000
Fault width perpendicular to strike (km)	80			Slide terminal velocity (m/s)	25.0	25.0
Shear modulus (Pa)	$4.5 \cdot 10^{10}$			Initial acceleration a_0 (m/s ²)	0.966	0.280

293

294 3.1.2. *Submarine landslide sources*

295 To simulate tsunami generation by the Gloria Knolls Slide and the potential collapse of the
296 Noggin Block, we used NHWAVE (Ma et al. 2013), a non-hydrostatic wave model that has
297 been successfully validated in laboratory settings (Enet and Grilli 2007; Tehranirad et al. 2012)
298 and has been used for several case studies of submarine mass failure-induced tsunamis (Tappin
299 et al. 2014; Grilli et al. 2015; Li et al. 2015; Schnyder et al. 2016). The code numerically
300 approximates the solutions to non-hydrostatic Navier-Stokes equations for incompressible flow
301 in three dimensions, implementing a terrain-following (i.e. sigma-layered) vertical coordinate
302 system. For simplicity and computational efficiency, a 3-dimensional, rigid, translational
303 failure was assumed for both cases, where the bottom boundary condition is dictated by a time-
304 varying change in depth imparted by an approximately Gaussian-shaped slide.

305
306 NHWAVE requires approximate landslide dimensions (i.e., length, width, thickness) to
307 construct the Gaussian-shaped slide that generates the initial tsunami. For both landslide cases,
308 these dimensions were determined in previous work (Puga-Bernabéu et al. 2013a, 2016, 2019),
309 and were thus adopted here (see Table 1). For the Gloria Knolls Slide, slide dimensions were
310 determined using bathymetry data containing the slide scar (Puga-Bernabéu et al. 2016, 2019).
311 The slide is believed to have failed sequentially in multiple phases, forming what is known as
312 a larger “slide complex”. Here, we modelled what was determined to be the worst-case scenario
313 of these failure phases (i.e., “Event 2, Worst-Case Scenario”, see Puga-Bernabéu et al., 2019).
314 This case was selected to represent one of the most severe submarine landslide cases for this
315 region, as the Gloria Knolls Slide is, thus far, the largest documented slide complex (total
316 volume $\approx 32 \text{ km}^3$) on the northeastern Australian margin (Puga-Bernabéu, in prep). For the
317 Noggin Block, the initial dimensions were determined from a rigorous, modelling-based slope
318 stability analysis conducted for the block (Puga-Bernabéu et al. 2013a). This feature is

319 comparatively small; the estimated slide volume is $\sim 0.77 \text{ km}^3$ (using the volume formulas of
320 Enet & Grilli, 2007). However, the block is relatively shallow, resting on the upper slope (\sim
321 400 m). An additional sensitivity analysis was conducted to test the impact of failure depth on
322 the initial tsunami wave height (see Section 4.2).

323

324 For both landslide cases, kinematic parameter a_0 was determined using the semi-empirical
325 formulations of Enet and Grilli (2007), and the peak slide velocity was prescribed a value of
326 25 m/s. This peak velocity is of similar magnitude to those recorded by submarine cable breaks
327 during the Grand Banks Event (i.e., 20-25 m/s; Fine et al., 2005). A landslide density of 2000
328 kg/m^3 was informed by sediment core measurements obtained by Ocean Drilling Program
329 (ODP) Leg 133 Site 819, which was drilled $\sim 70 \text{ km}$ north of the Noggin Block and the Gloria
330 Knolls Slide (Davies et al. 1991). Each simulation was run for a landslide failure duration of 3
331 minutes at 100 m resolution horizontally and at 5 sigma layers vertically.

332

333

334 3.2. Tsunami propagation

335 The resulting ocean free surface elevations, as well as the depth-averaged zonal and meridional
336 velocities, were smoothed and re-interpolated from the tsunami generation model outputs to
337 set the initial conditions for the wave propagation model. Tsunami propagation was modelled
338 using FUNWAVE-TVD (Shi et al. 2012), a widely-used, fully nonlinear Boussinesq tsunami
339 propagation code that has been validated against NOAA's National Tsunami Mitigation
340 Program benchmark requirements (NTHMP, 2012). The model captures wave behaviours such
341 as shoaling, dissipation via bottom friction and wave breaking, and frequency dispersion (Shi
342 et al. 2012).

343

344 For the earthquake scenarios, tsunami propagation was simulated across the Coral Sea using a
345 1 arcminute ETOPO1 grid (Amante and Eakins 2009). Smaller nested grids of 200 x 200 m
346 resolution were used to resolve the earthquake-generated waves upon arrival to the continental
347 shelf. These grids were generated from a 100 m resolution bathymetric dataset spanning the
348 entire northeastern Australian margin, including the GBR (i.e. “3DGBR”, Beaman, 2010; see
349 Figure 3a). Waves were introduced into the smaller nested grids via a one-way coupling
350 scheme. Near-field landslide scenarios were also simulated with grids generated from the
351 3DGBR bathymetric dataset. Bathymetry for all cases was smoothed using a Gaussian filter to
352 prevent numerical instability incited by steep bathymetric slopes.

353

354 The spatial resolution of the model domains was carefully selected using a range of sensitivity
355 analyses (see Online Resource 2). For the earthquake scenarios, a 200 x 200 m grid is deemed
356 sufficient to resolve interactions between the propagating waves and the seafloor. The Gloria
357 Knolls Slide and the Noggin Block potential failure necessitated finer resolution grids to
358 adequately resolve shoaling and scattering processes (100 m and 50 m resolution, respectively).

359

360 It is important to note here that although Geowave also has the ability to simulate tsunami
361 generation and propagation by both coseismic slip and landslide sources, we opted to use
362 updated models that more explicitly resolve processes involved in landslide tsunami generation
363 (i.e. the non-hydrostatic formulations of NHWAVE) and more accurately represent frequency
364 dispersion of propagating gravity waves (i.e. the improved fully-nonlinear, Boussinesq
365 formulations of FUNWAVE-TVD). Dispersive effects become more critical to simulate for
366 far-field and landslide tsunami sources (Tehranirad et al. 2015).

367

368 3.3. Run-up estimation

369 In the absence of the nearshore high-resolution bathymetric and topographic data (<50 m)
370 required to accurately resolve onshore tsunami inundation, final estimated run-up distributions
371 were calculated using virtual tide gauges placed along the shoreline in ~25 m water depth d
372 using the following equation:

373
$$R = A(d)^{\frac{4}{5}} \cdot d^{\frac{1}{5}} \quad (\text{Eq.1})$$

374

375 where R is the estimated run-up and $A(d)$ is the maximum wave amplitude at a virtual gauge
376 location at depth d . This formula is based on the conservation of wave energy flux and applies
377 to both breaking and non-breaking waves (Ward and Asphaug 2003).

378

379 3.4. Testing the impact of the GBR on tsunami propagation

380 A major objective of this study is to test whether the structural complexity of the GBR plays a
381 role in attenuating tsunami wave energy. The GBR exhibits structural complexity at two
382 predominant spatial scales. Firstly, due to the morphological diversity of individual species,
383 coral cover is structurally complex on the meter to sub-meter scale (Nelson 1996; Graham and
384 Nash 2013). We hereafter refer to the structural complexity of coral cover as “ecosystem-scale”
385 complexity. In a modelling context, this “ecosystem-scale” complexity cannot be resolved in
386 the computational domain and must be parameterized (see Section 3.4.1). Secondly, the GBR
387 exhibits structural complexity at the >1 km scale. The reef structure itself is composed
388 primarily of completely submerged or semi-submerged carbonate platforms. These features
389 create complex positive relief on the submerged continental shelf, and much of this relief (aside
390 from smaller, deeper pinnacles and terraces), is resolved by the 100 m-resolution 3DGBR
391 bathymetric dataset (Beaman 2010). Thus, the reef structure can be adequately resolved in the

392 computational domain. We hereafter refer to complexity introduced by the reef structure as
393 “bathymetric-scale” complexity.

394

395 The following sections detail how the impact of GBR’s structural complexity at both the
396 ecosystem-scale and bathymetric-scale was tested.

397

398 3.4.1. *Ecosystem-scale complexity: coral cover parameterization*

399 In FUNWAVE-TVD, bottom shear stress τ is calculated using the standard quadratic drag law
400 (Shi et al. 2016):

401

$$402 \quad \tau = \frac{1}{2}\rho C_D U^2 \quad (\text{Eq.2})$$

403 where C_D is the non-dimensional bottom friction coefficient, ρ is the density of water, and U
404 is the particle velocity at the seabed. A variable bottom friction coefficient was established
405 throughout the domain, where it was altered according to the presence or absence of coral cover
406 on reef platforms. A value of $C_D=0.1522$ was prescribed to reef platforms to simulate coral
407 cover (average depth of platforms ≈ 14.9 m). This value was obtained from a prior field
408 investigation of the hydraulic roughness of coral reefs, which was conducted at John Brewer
409 Reef, a reef platform within the GBR that lies close to the study region (Nelson, 1996; ~ 80 km
410 from the computational domain). Additionally, this coefficient falls well within the range of
411 values obtained for other reefs (Monismith et al. 2013). All other areas of the computational
412 domain where prescribed the conventional value of $C_D = 0.0025$, which is representative of
413 sand-covered seafloor (Grilli et al. 2015). This approach was used to create the “coral cover”
414 scenarios, where the ecosystem-scale structural complexity of the GBR was taken into account
415 in tsunami propagation simulations (Figure 3a).

416

417 To test the impact of coral cover on tsunami attenuation, the “coral cover” scenarios were then
418 compared to “smooth platform” scenarios, where coral cover was effectively removed. In the
419 “smooth platform” scenarios, all areas of the bottom boundary, reef platforms included, were
420 prescribed a standard bottom friction coefficient value of $C_D = 0.0025$.

421

422 3.4.2. Bathymetric-scale complexity: testing the impact of the reef platforms

423 Larger-scale, bathymetric complexity is introduced by the reef structure itself, which is
424 composed primarily of reef platforms. Testing the impact of these platforms on tsunami
425 propagation requires artificial bathymetry, where the positive relief formed by the platforms is
426 removed from the shelf (Figure 3b). Platforms were removed by “cookie-cutting” the
427 bathymetry, removing areas of the mid- to outer-shelf containing the reef platforms. The
428 bathymetry was then linearly interpolated and smoothed over the cookie-cut areas employing
429 a Gaussian filter. This modified bathymetry was then used in the “no reef platforms” scenarios.

430

431 3.5. Testing the additional effect of tidal phase

432 As the central northeastern Australian margin is a meso-tidal environment, water depths over
433 the reef platforms can vary significantly over several hours. Consequently, tidal phase has been
434 shown to modulate the degree of wind wave attenuation (Young and Hardy 1993). To test the
435 impact of tidal phase on tsunami propagation, two additional scenarios were configured: one
436 where the highest spring tide (+1.75 m above MSL) and one where the lowest spring tide (-
437 1.75 m above MSL) coincided with tsunami arrival at the GBR.

438

439

440

441 **4. Results**

442

443 4.1. Earthquake tsunami generation and regional propagation

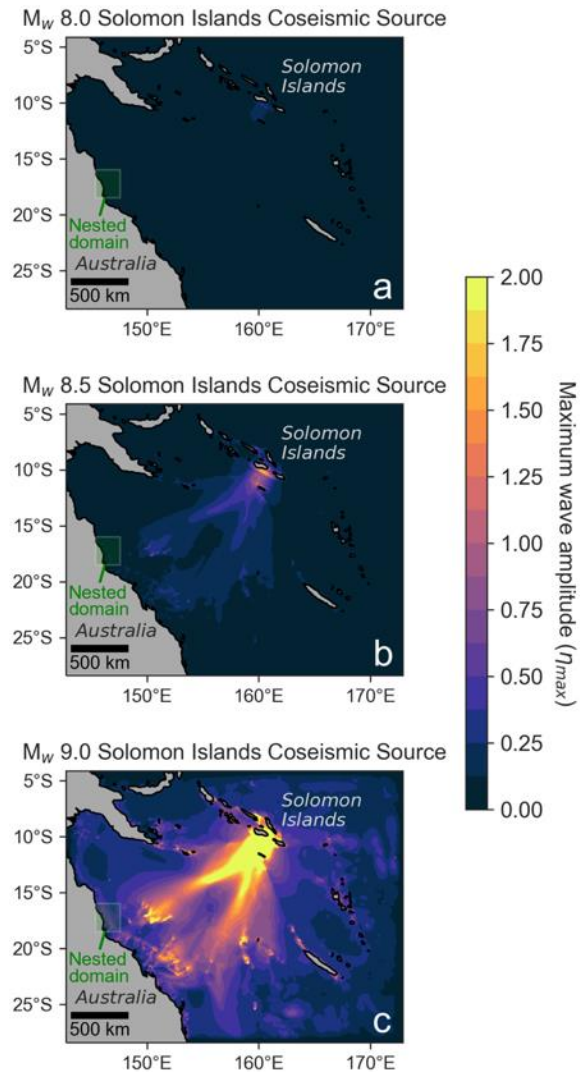
444 For the hypothetical M_w 8.0, 8.5, and 9.0 Solomon Islands earthquake scenarios, the generation
445 model simulates initial peak wave amplitudes of 0.32 m, 1.7 m, and 9.7 m, respectively (Figure
446 4). The tsunamis in each case then propagate across the Coral Sea to the outer GBR margin
447 after an approximately 3.5 hour travel time, which is consistent with previous travel times
448 observed for the Solomon Islands source-zone (NGDC/WDS 2020). Upon arrival to the outer
449 Australian continental shelf within the nested domain, wave amplitudes range from ~1-2 cm
450 for the M_w 8.0 case, ~6-10 cm for the M_w 8.5 case, and ~30-60 cm for the M_w 9.0 case.

451

452

453

Draft manuscript



454

455 **Figure 4.** Maximum wave amplitudes simulated by FUNWAVE-TVD for the hypothetical M_w 8.0 (a), M_w 8.5
 456 (b), M_w 9.0 (c) Solomon Islands earthquake sources. Initial maximum wave amplitudes at the source are 0.32 m,
 457 1.7 m, and 9.7 m, respectively. The simulated propagation time represented here is \sim 8 hours to allow waves to
 458 reach all parts of the bathymetric domain.

459

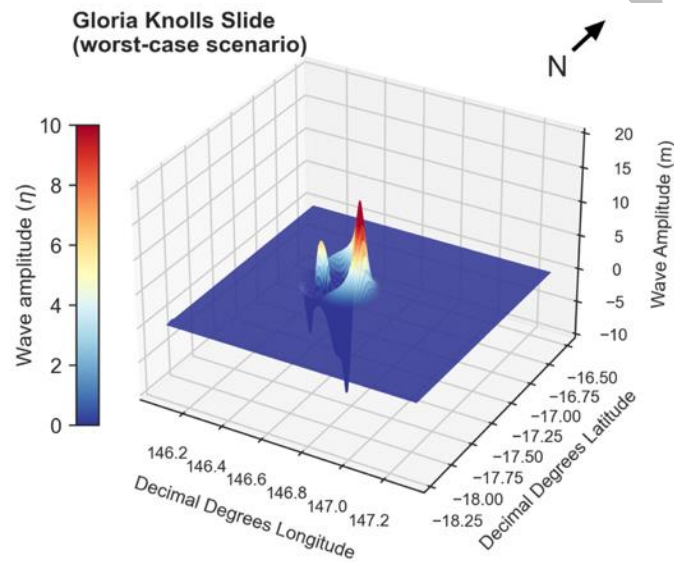
460 4.2. Landslide tsunami generation

461 The landslide generation model NHWAVE simulates \sim 18 m-high seaward-propagating wave
 462 crest and \sim 9 m-high landward-propagating wave crest for the Gloria Knolls Slide (Figure 5),
 463 assuming the previously-determined worst-case scenario (Puga-Bernabéu et al. 2019). For the
 464 potential collapse of the Noggin Block, the landslide generation model simulates a \sim 1.3 m-high
 465 seaward-propagating crest and a \sim 3.5 m-high landward-propagating crest (Figure 6a).
 466 Sensitivity analyses indicate that initially generated wave amplitudes are responsive to

467 moderate changes in depth (+/- 100 m). If the block was to initially fail 100 m deeper (500 m
468 depth), the wave amplitude of the landward-propagating crest reaches ~ 2.5 m, about 71% of
469 its original value. On the other hand, should the block fail at a 100 m-shallower depth (300 m
470 depth), the wave amplitude peaks at ~4.8 m, growing roughly 37%. For the subsequent
471 simulations of tsunami propagation, the main Noggin Block scenario (failure depth = 400 m)
472 is implemented.

473

474

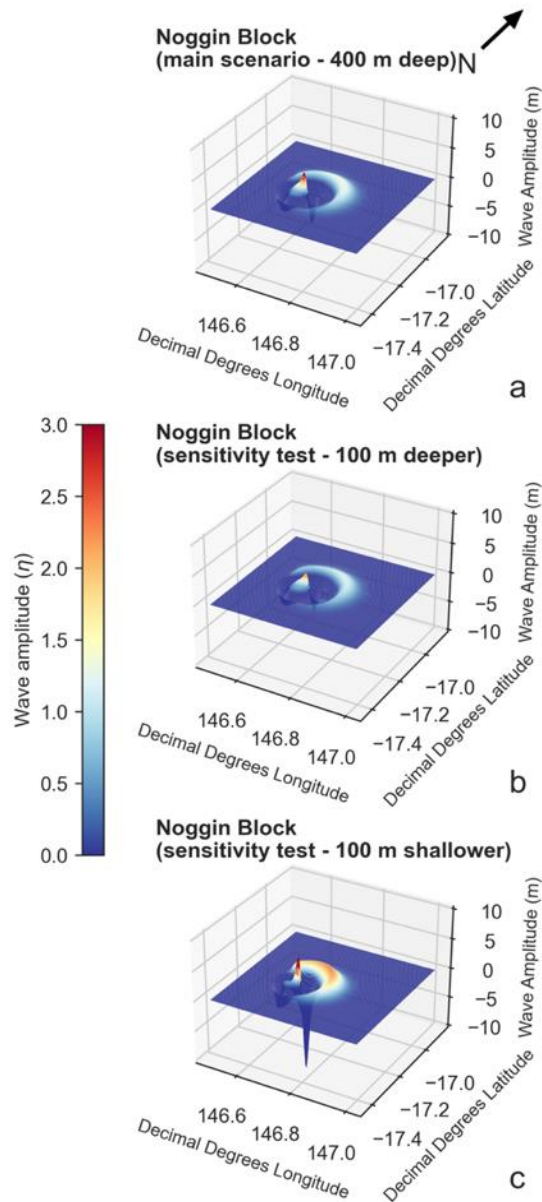


475

476 **Figure 5.** Instantaneous free surface elevation at $t = 9$ min for the Gloria Knolls landslide tsunami scenario,
477 simulated using NHWAVE. Wave amplitude peaks at $\eta \approx 18$ m. The smaller peak is the landward-propagating
478 wave, and it peaks at $\eta \approx 9$ m.

479

480



481

482 **Figure 6.** Instantaneous free surface elevations at $t = 9$ min for the potential Noggin Block collapse, simulated
 483 using NHWAVE. The main scenario (a) assumes a failure depth of ~ 400 m, where the peak wave amplitude for
 484 the landward-propagating crest reaches ~ 3.5 m. A sensitivity test indicates that a 100 m-deeper failure (b) would
 485 result in a substantially smaller wave crest ($\eta_{\max} \approx 2.5$ m, 71% of its original value). A 100 m-shallower failure
 486 (c) would result in a larger initial wave crest ($\eta_{\max} \approx 4.8$ m, 37% greater than its original value).

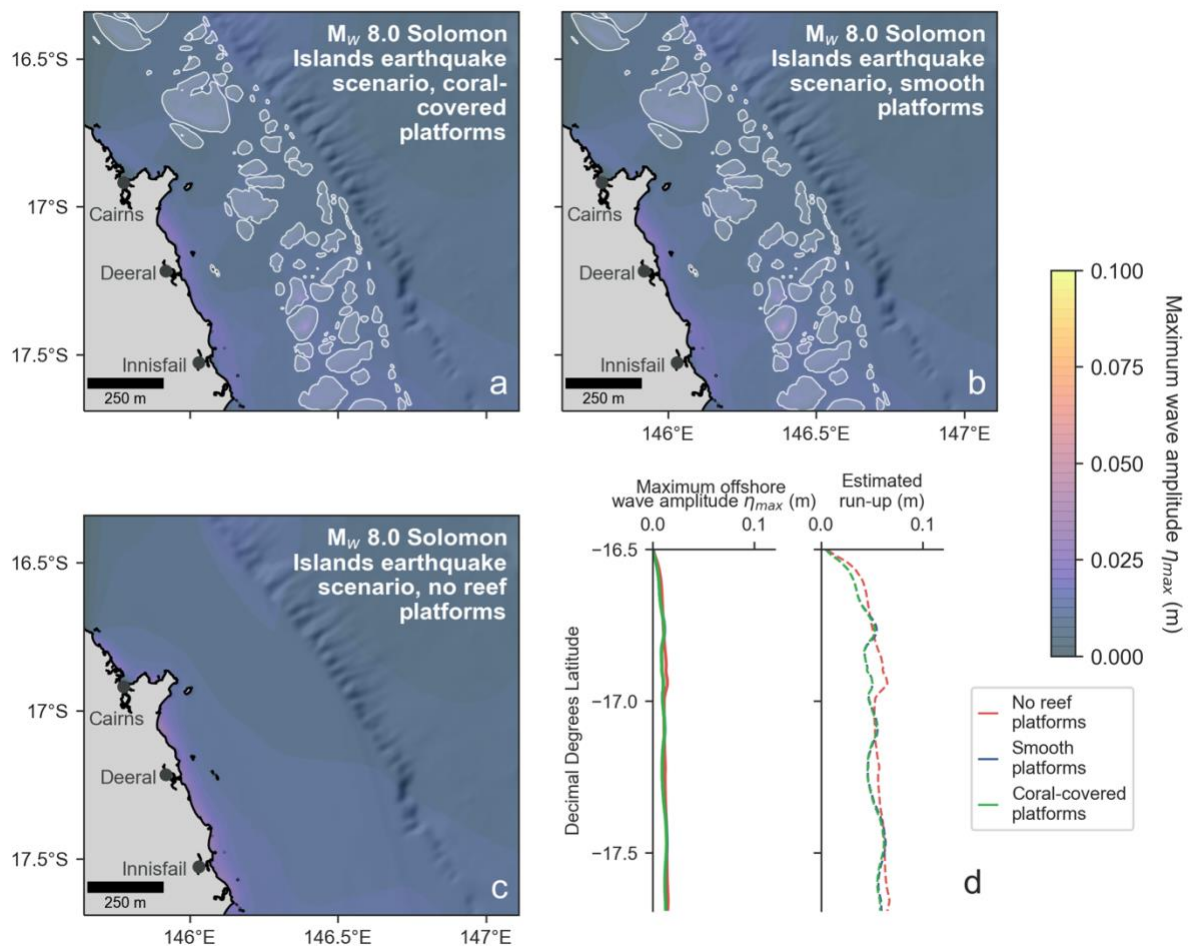
487

488 4.3. Nearshore earthquake tsunami propagation

489 Results indicate that the GBR's buffering impact on the earthquake-generated tsunami, which
 490 originates in the Solomon Islands source-zone, depends on the magnitude of the initial
 491 earthquake. Turning firstly to the hypothetical M_w 8.0 earthquake scenario (Figure 7a),

492 maximum wave amplitudes across the domain remain under 5 cm when coral cover is present
 493 atop the reef platforms (i.e. when ecosystem-scale complexity is high), where maximum
 494 estimated run-up R_{\max} reaches ~ 6.2 cm. When coral cover is removed (Figure 7b), maximum
 495 wave amplitudes increase marginally or remain the same, growing 2% on average along the 25
 496 m isobath (Figure 7c). Estimated run-ups follow a similar trend ($R_{\max} \approx 6.4$ cm). Finally, when
 497 reef platforms are removed from bathymetry (Figure 7c), offshore wave amplitudes increase a
 498 bit more substantially (17% on average), but still fall below ~ 5 cm across the domain. The
 499 maximum run-up estimate remains at a similar elevation ($R_{\max} \approx 6.7$ cm, Figure 7d).

500



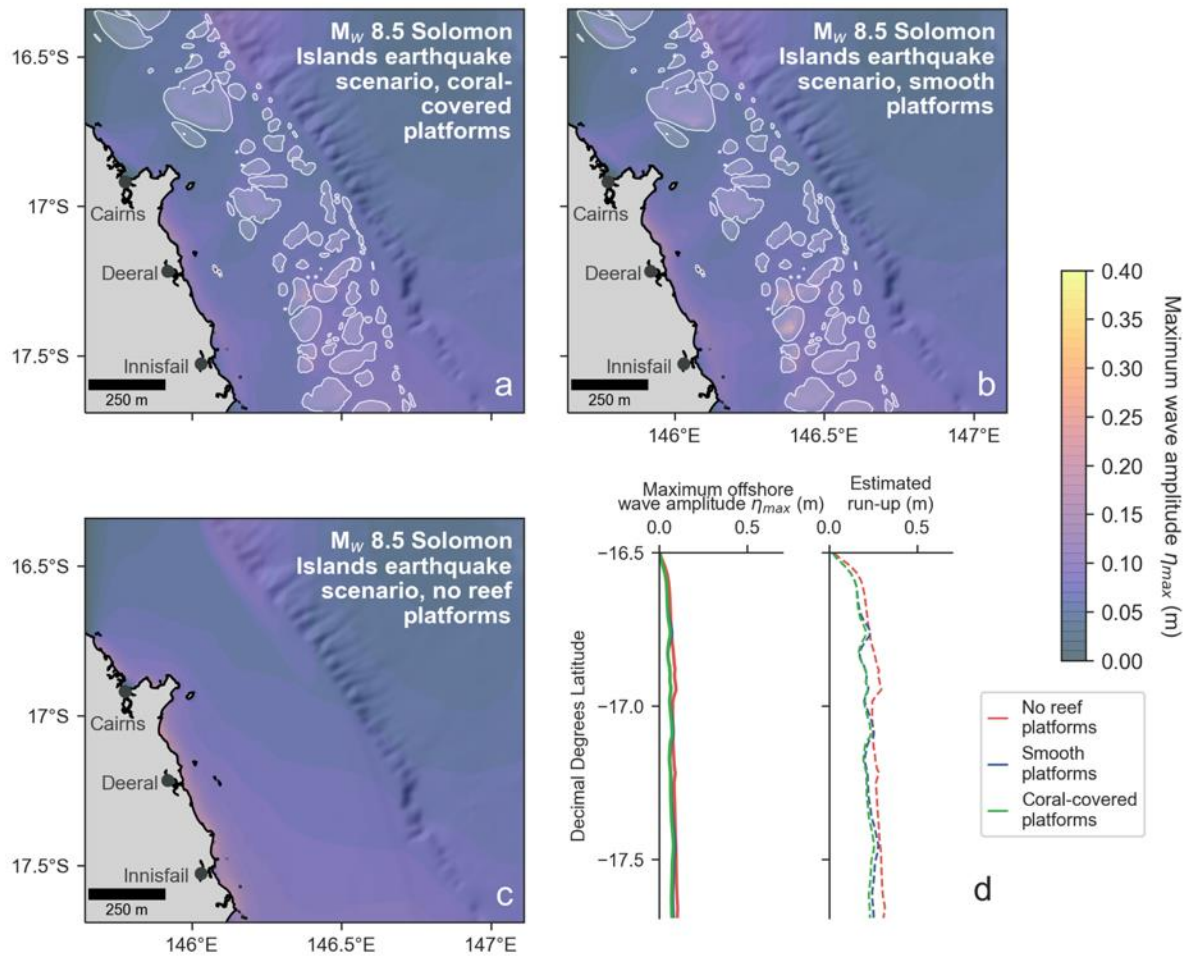
501

502 **Figure 7.** Maximum wave amplitude distributions for the hypothetical M_w 8.0 Solomon Islands earthquake
 503 scenario simulated with a) the modern “coral-covered platforms” (bottom friction coefficient $C_D=0.1522$ on
 504 platforms, shown in white) b) “smooth platforms” ($C_D=0.0025$), and c) “no reef platforms”. d) Corresponding
 505 maximum offshore wave amplitude and estimated run-up distributions. Maximum run-up estimates are 6.2 cm

506 for the “coral-covered platforms” scenario, 6.4 cm for the “smooth platforms” scenario, and 6.7 cm for the “no
507 reef platforms” scenario. Offshore wave amplitudes were interpolated along the 25 m isobath.

508

509 For the hypothetical M_w 8.5 Solomon Islands earthquake scenario, the GBR, both in terms of
510 its ecosystem-scale and bathymetric scale complexity, appears to have slightly more impact on
511 offshore tsunami amplitudes and estimated run-up. When coral cover is present (Figure 8a),
512 wave amplitudes landward of the GBR range from ~5-10 cm, with an R_{max} estimate of ~26 cm.
513 When platforms are smoothed (Figure 8b), these amplitudes grow, increasing 7% on average
514 along the 25 m isobath. The maximum run-up estimate also increases slightly ($R_{max} \approx 28$ cm).
515 Wave amplitudes similarly increase when reef platforms are removed (Figure 8c; 13% average
516 increase along the 25 m isobath; $R_{max} \approx 32$ cm). Overall, the changes in the amplitude and run-
517 up distributions are moderate for this case (Figure 8d).



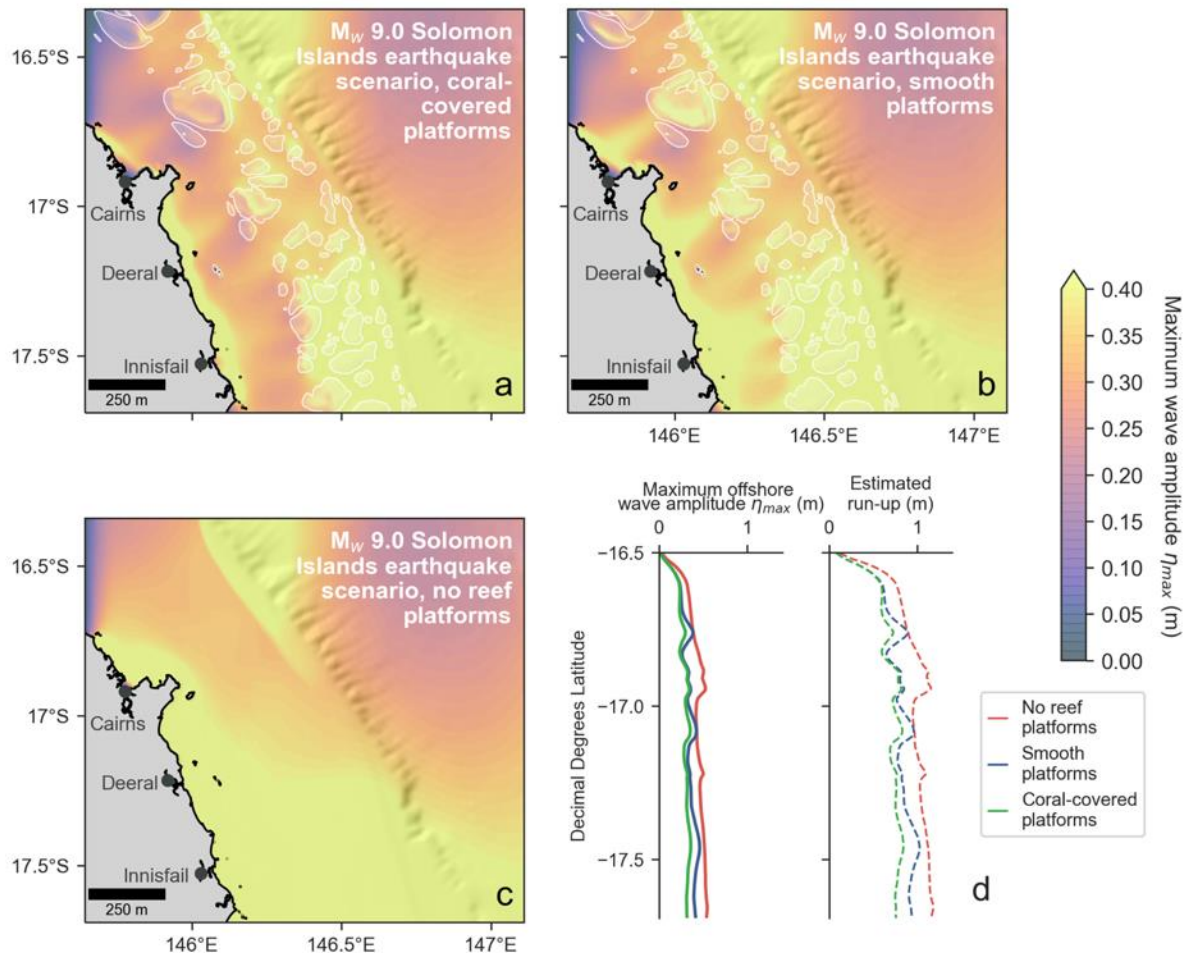
518

519 **Figure 8.** Maximum wave amplitude distributions for the hypothetical M_w 8.5 Solomon Islands earthquake
 520 scenario simulated with a) the modern “coral-covered platforms” (bottom friction coefficient $C_D=0.1522$ on
 521 platforms, shown in white) b) “smooth platforms” ($C_D=0.0025$), and c) “no reef platforms”. d) Corresponding
 522 maximum offshore wave amplitude and estimated run-up distributions. Maximum run-up estimates are 26 cm for
 523 for the “coral-covered platforms” scenario, 28 cm for the “smooth platforms” scenario, and 32 cm for the “no reef
 524 platforms” scenario. Offshore wave amplitudes were interpolated along the 25 m isobath. For animations of
 525 tsunami propagation for the “coral-covered platforms” and “no reef platforms” scenarios, see Online Resources 3
 526 and 4.

527

528 The GBR has a much more substantial impact on the propagating tsunami when considering
 529 the hypothetical M_w 9.0 Solomon Islands earthquake source. Overall, the M_w 9.0-generated
 530 tsunami is significantly larger in amplitude than its smaller-magnitude counterparts. When
 531 coral cover is present on reef platforms, maximum offshore wave amplitudes range from about
 532 0.2-0.4 m landward of the GBR (Figure 9a), resulting in a maximum estimated run-up of ~ 0.85
 533 m. When platforms are smoothed (Figure 9b), amplitudes increase (18% on average along the
 534 25 m isobath), particularly directly landward of broad reef platforms. Likewise, the maximum

535 estimated run-up increases when platforms are smoothed, reaching 1 m. Finally, when reef
 536 platforms are removed from bathymetry, amplitudes increase substantially on the shelf (51%
 537 on average along the 25 m isobath), leading to a maximum estimated run-up of ~1.2 m (Figure
 538 9d).



539

540 **Figure 9.** Maximum wave amplitude distributions for the hypothetical M_w 9.0 Solomon Islands earthquake
 541 scenario simulated with a) the modern “coral-covered platforms” (bottom friction coefficient $C_D=0.1522$ on
 542 platforms, shown in white) b) “smooth platforms” ($C_D=0.0025$), and c) “no reef platforms”. d) Corresponding
 543 maximum offshore wave amplitude and estimated run-up distributions. Maximum run-up estimates are 0.85 m
 544 for the “coral-covered platforms” scenario, 1.0 m for the “smooth platforms” scenario, and 1.2 m for the “no reef
 545 platforms” scenario. Offshore wave amplitudes were interpolated along the 25 m isobath.

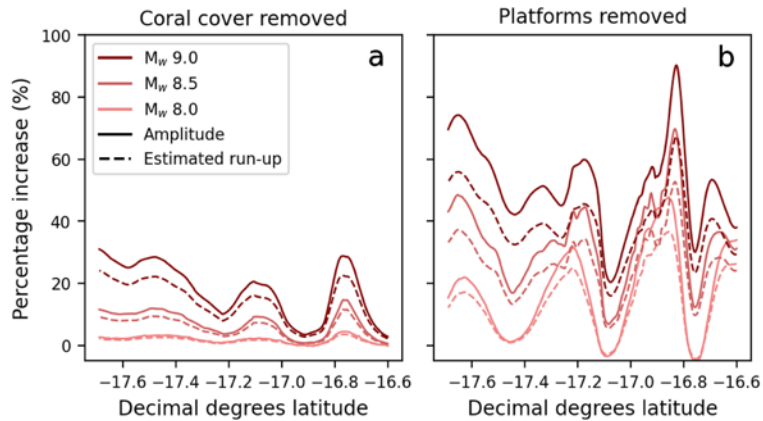
546

547 Figure 10 shows the percentage increase exhibited by both offshore wave amplitude and
 548 predicted run-up when both the ecosystem-scale and bathymetric-scale complexity of the GBR
 549 is removed. This gives an indication of the relative degree to which the GBR attenuates tsunami
 550 wave energy. Firstly considering ecosystem-scale complexity isolation, when coral cover is

551 removed, under the M_w 8.0 scenario (Figure 10a), wave amplitudes are slightly larger on a
552 percentage-wise basis compared to when coral cover is present, ranging from 0-4% increase
553 within the study area. For the M_w 8.5 scenario, this percentage increase heightens, ranging from
554 1-15%. Finally, for the largest earthquake scenario (M_w 9.0), amplitudes increase substantially,
555 ranging from 3-31% higher compared to when coral cover is present. Percentage increases in
556 the estimated run-up distributions follow similar patterns. Amplitude and run-up increases are
557 highly variable alongshore, with the largest peaks occurring directly behind shelf areas with
558 broad, shallow reef platforms. For instance, the city of Cairns (latitude $\approx 16.8^\circ\text{S}$) seems to
559 benefit from being situated behind a wide, shallow reef platform that lies in the path of the
560 tsunami. The overall trend indicates that the attenuating effect of coral cover increases with the
561 magnitude of the earthquake source.

562
563 The second panel of Figure 10 reflects the very substantial combined attenuative impact of
564 ecosystem-scale and bathymetric-scale complexity (i.e. coral cover and reef platforms). When
565 coral cover and reef platforms are removed, wave amplitudes and run-ups increase
566 considerably for the M_w 8.0 scenario (range: 0-48%). Notably, at a few locations, this
567 percentage dips marginally below zero (-5% maximum), indicating that these areas would
568 experience a *decrease* in offshore amplitudes and estimated run-ups if reef platforms were not
569 present. Amplitude and run-up distributions follow a similar pattern, increasing overall for the
570 M_w 8.5 (range: 7-70%), and again for the M_w 9.0 (range: 20-90%). These results reflect the
571 significant combined attenuative impact of both coral cover and the reef platforms on the
572 propagating tsunamis, which increases with earthquake source magnitude. We again note the
573 immense variability of the amplitude and run-up increases alongshore for each earthquake
574 scenario.

575



576

577 **Figure 10.** Percentage increases in both earthquake tsunami amplitude and estimated run-up when a) coral cover
 578 is removed and b) reef platforms are removed. Amplitudes, which were also used to calculate run-up, were
 579 extracted along the 25 m isobath.

580

581 For all cases, the first tsunami waves arrive at the coast after an approximately 4 hr travel time
 582 from the Solomon Islands source-zone. When passing over the shelf, the tsunami experiences
 583 diffraction, shoaling, and focusing. In particular, broad, moderately deep platforms tend to
 584 focus tsunami wave energy towards shore (e.g., Figure 9b). When platforms are removed, this
 585 behaviour disappears. For animations of the Mw 8.5 scenario simulated with coral cover and
 586 no reef platforms, see Online Resources 3 and 4.

587

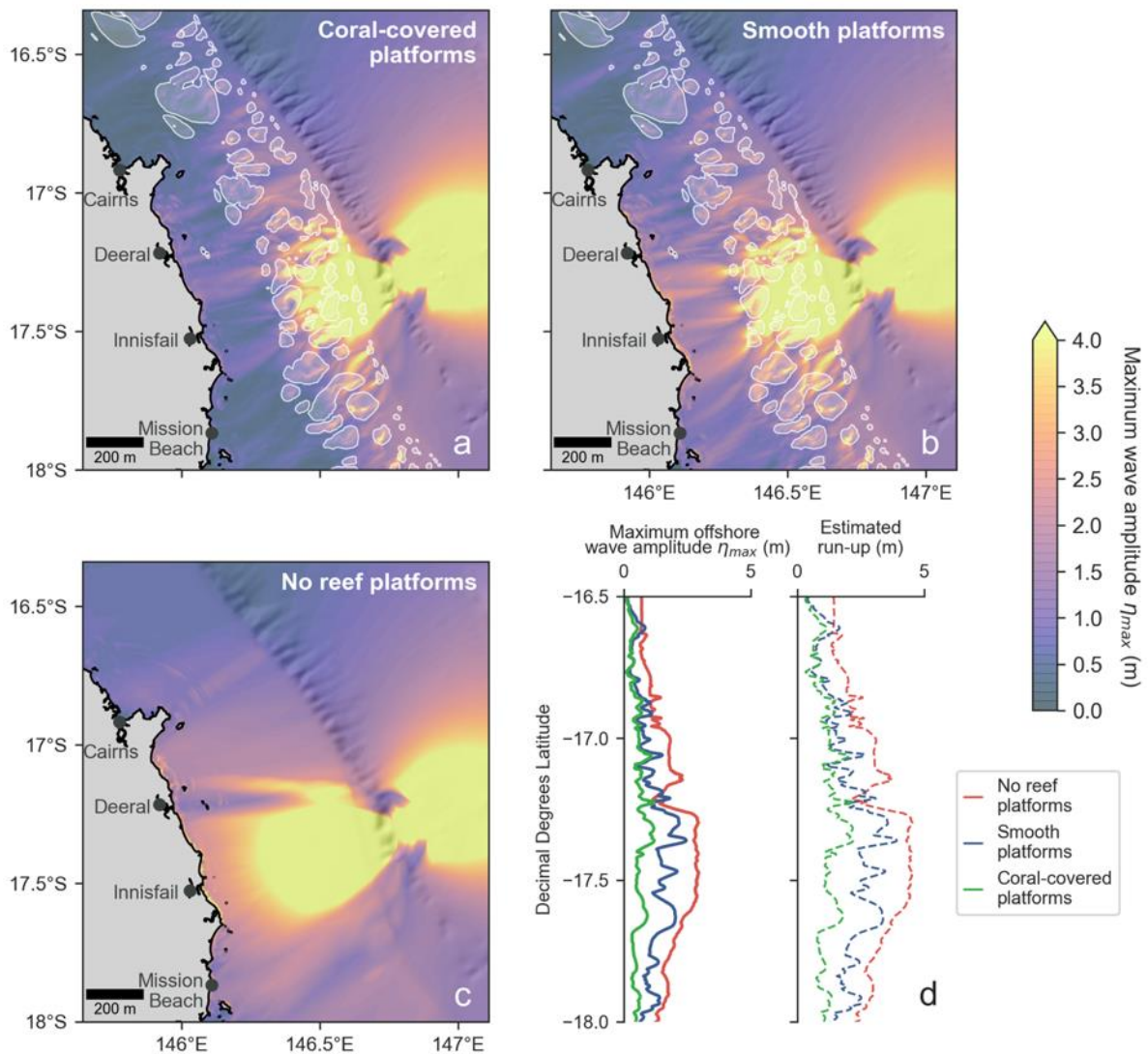
588 4.4. Nearshore landslide tsunami propagation

589 Simulations indicate that the impact of ecosystem-scale and bathymetric-scale complexity on
 590 tsunami attenuation is sizeable for the landslide-generated cases considered on this margin.

591 Turning firstly to the previously-termed “worst-case scenario” for the Gloria Knolls Slide
 592 (Puga-Bernabéu et al. 2016), when reef platforms are covered by coral, offshore amplitudes
 593 markedly decline from over ~4 m to under ~2 m landward of the platforms (Figure 11a), and
 594 maximum estimated run-up is estimated reaches up to ~2.2 m. When coral cover is removed
 595 (Figure 11b), offshore amplitudes along the 25 m isobath nearly double, increasing by a factor
 596 of ~1.9 on average. Maximum estimated run-up rises to ~3.9 m under the “smooth platforms”

597 simulation. When reef platforms are removed (Figure 11c), offshore amplitudes more than
 598 quadruple on average (fold-change: ~ 4.6), when compared to the “coral-covered platforms”
 599 scenario. When platforms are absent, estimated maximum run-up increases again, reaching 4.6
 600 m (Figure 11d). The total elapsed time between tsunami generation and the arrival of the first
 601 waves is ~ 1.5 hrs.

602



603

604 **Figure 11.** Maximum wave amplitude distributions for the Gloria Knolls Slide (worst-case scenario) simulated
 605 with a) the modern “coral-covered platforms” (bottom friction coefficient $C_D=0.1522$ on platforms, shown in
 606 white) b) “smooth platforms” ($C_D=0.0025$), and c) “no reef platforms”. d) Corresponding maximum offshore
 607 wave amplitude and estimated run-up distributions. Maximum run-up estimates are ~ 2.2 m for the “coral-
 608 covered platforms” scenario, ~ 3.9 m for the “smooth platforms” scenario, and ~ 4.6 m for the “no reef
 609 platforms” scenario. Offshore wave amplitudes were interpolated along the 25 m isobath. For animations of the
 610 “coral-covered platforms” and “no reef platforms” scenarios, see Online Resources 5 and 6.

611

612

613 Results for the Noggin Block potential slide are very similar to that of the Gloria Knolls Slide,
614 though it produces a smaller tsunami (see Section 4.2). Assuming healthy reef growth (Figure
615 12a), offshore amplitudes remain under ~1 m, where they sharply decline upon passing over
616 the GBR platforms. Maximum estimated run-up for this scenario is ~1.4 m. When coral cover
617 is removed (Figure 12b), offshore amplitudes along the 25 m isobath increase by a factor of ~2
618 on average, with the maximum run-up rising to 1.8 m. Finally, when platforms are removed
619 from the simulations (Figure 12c), offshore amplitudes along the 25 m isobath are, on average,
620 4.5 times larger than the original “coral cover” scenario. Peak estimated run-up reaches ~2.8
621 m under the “no reef platforms” scenario (Figure 12d). The total time between tsunami
622 generation and the arrival of the first waves is similar to the Gloria Knolls landslide tsunami
623 (~1.5 hrs).

624

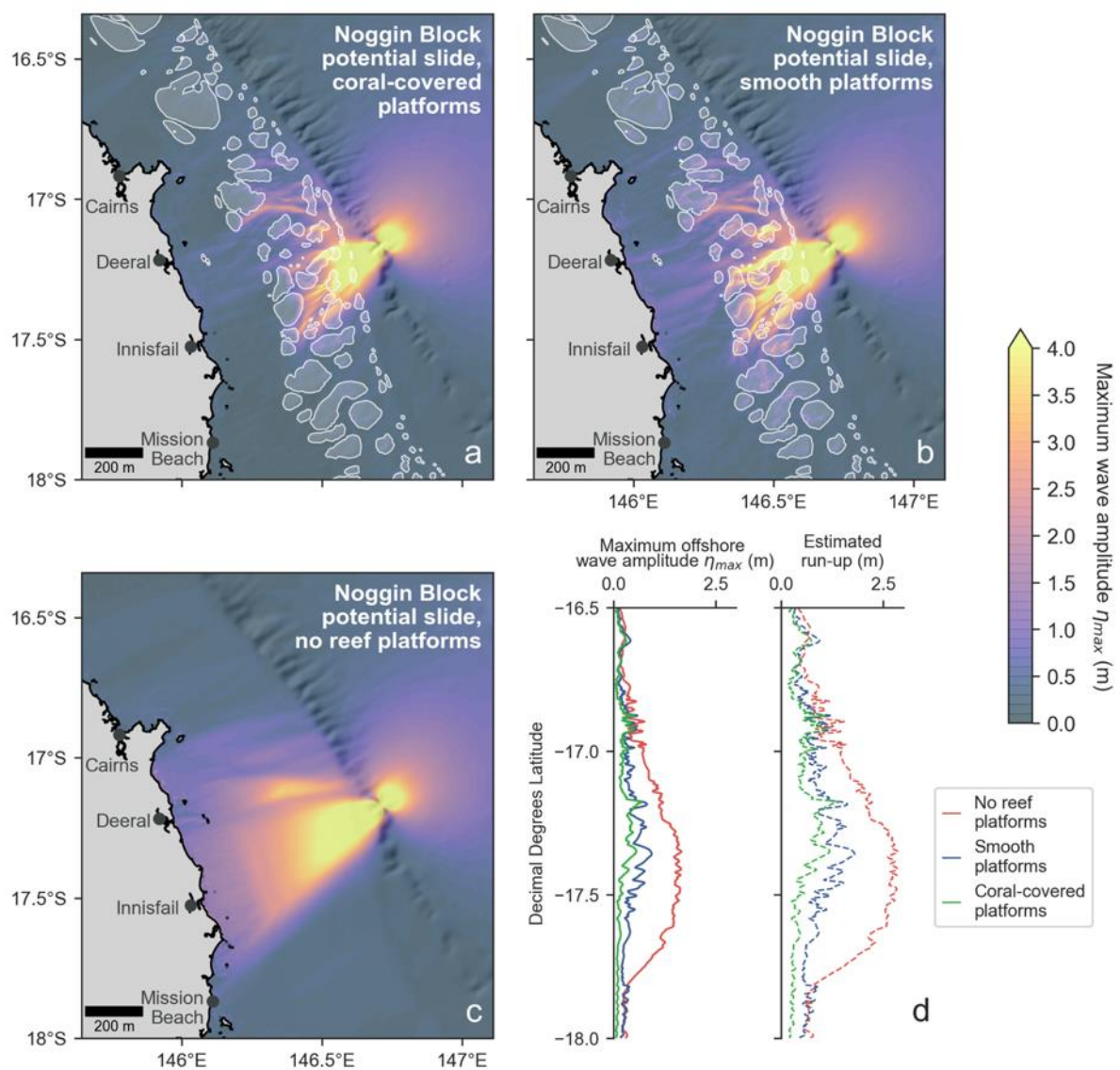
625 Figure 10 shows the overall change in offshore wave amplitude and estimated-runup when
626 coral cover and reef platforms are removed from simulations, this time represented in terms of
627 fold-change rather than percentage change. For each landslide case, offshore amplitudes along
628 the 25 m isobath, along with estimated run-ups, tend to double when coral cover is removed
629 (Figure 10a). When platforms are removed, the amplitudes and run-ups increase significantly
630 for each case, but more so for the Noggin Block potential slide (Figure 10b). Again, we
631 highlight the enormous along-shore variability in amplitude and run-up change across
632 simulations.

633

634 Landslide tsunamis across both cases exhibit common behaviours. Amplitude and run-up
635 distributions follow a localized bell-curve due to radial damping, a standard process undergone

636 by point-source tsunamis (Brune et al., 2010; Harbitz et al., 2006). Additionally, reef platforms
 637 greatly interfere with these comparably shorter waves as they traverse the shallow continental
 638 shelf (Harbitz et al., 2006). For animations of both the Gloria Knolls slide scenario simulated
 639 with coral-covered platforms and no reef platforms, see Online Resources 5 and 6. For the
 640 same corresponding Noggin Block landslide tsunamis, see Online Resources 7 and 8.

641
 642

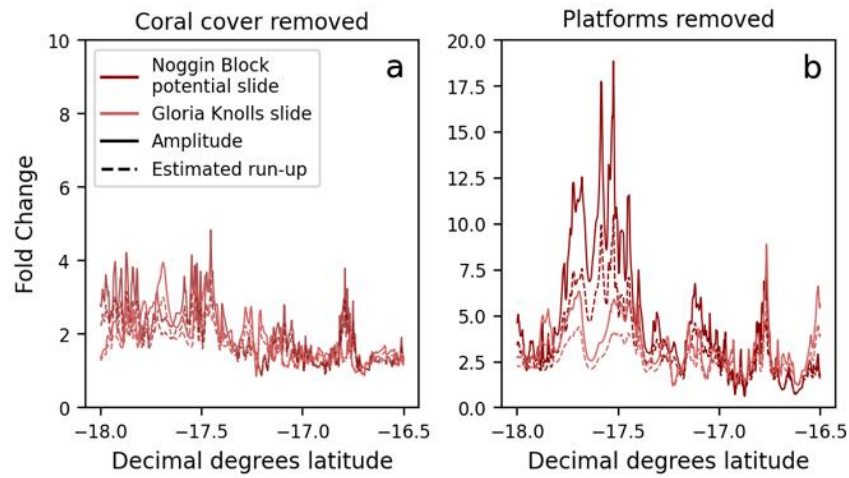


643

644 **Figure 12.** Maximum wave amplitude distributions for the Noggin Block potential landslide scenario simulated
 645 with a) the modern “coral-covered platforms” (bottom friction coefficient $C_D=0.1522$ on platforms, shown in
 646 b) “smooth platforms” ($C_D=0.0025$), and c) “no reef platforms”. d) Corresponding maximum offshore
 647 wave amplitude and estimated run-up distributions. Maximum run-up estimates are ~1.4 m for the “coral-covered
 648 platforms” scenario, ~1.8 m for the “smooth platforms” scenario, and ~2.9 m for the “no reef platforms” scenario.

649 Offshore wave amplitudes were interpolated along the 25 m isobath. For animations of the “coral-covered
650 platforms” and “no reef platforms” scenarios, see Online Resources 7 and 8.

651
652



653

654 **Figure 13.** Fold-change increase in both landslide tsunami amplitude and estimated run-up when a) coral cover
655 is removed and b) reef platforms are removed. Amplitudes, which were also used to calculate run-up, were
656 extracted along the 25 m isobath.

657

658

659 4.5. Tidal impacts on tsunami propagation

660 The additional impact of tide level was tested for the M_w 8.5 Solomon Islands earthquake
661 scenario, the Gloria Knolls Slide scenario, and the Noggin Block potential slide scenario.

662 Results indicate a minimal impact of tide level on the degree of attenuation of the M_w 8.5
663 earthquake-triggered tsunami (Figure 14a), where amplitudes were 1.6% lower on average at

664 low spring tide (1.75 m below MSL; Figure 14b) and 2.6% higher on average at high spring
665 tide (1.75 m above MSL; Figure 14c). Offshore amplitude and run-up distributions along the

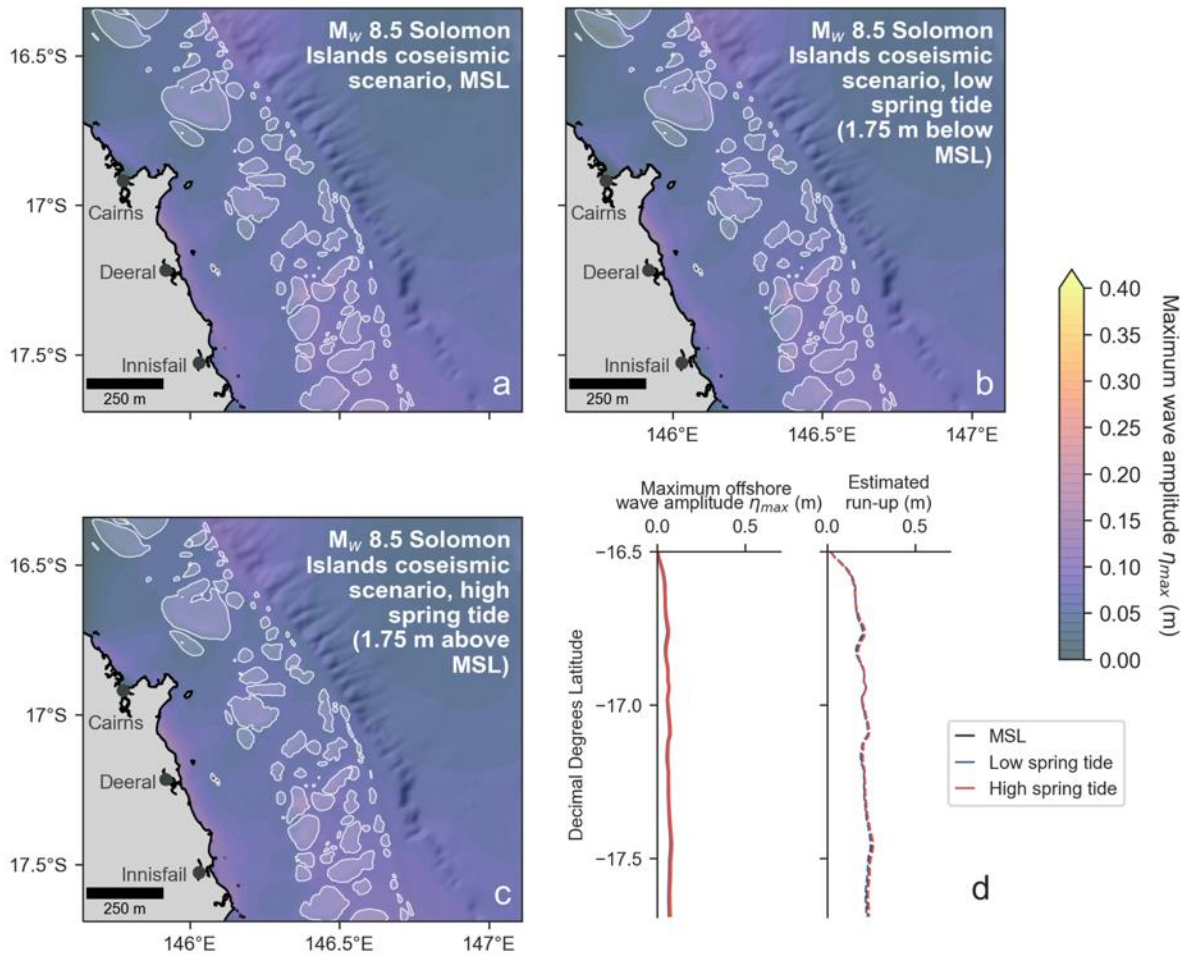
666 25 m isobath are very similar for all tide cases (Figure 14d). For the Gloria Knolls Slide, the
667 effect of tides is more pronounced, where amplitudes decrease 11 % on average during low

668 spring tide and increase 17% on average at high spring tide (Figure 15). Similarly, for the

669 Noggin Block, potential slide scenario (Figure 16a), amplitudes were 16% lower on average at

670 low spring tide (Figure 16b) and 6% higher on average at high spring tide (Figure 16c).

671

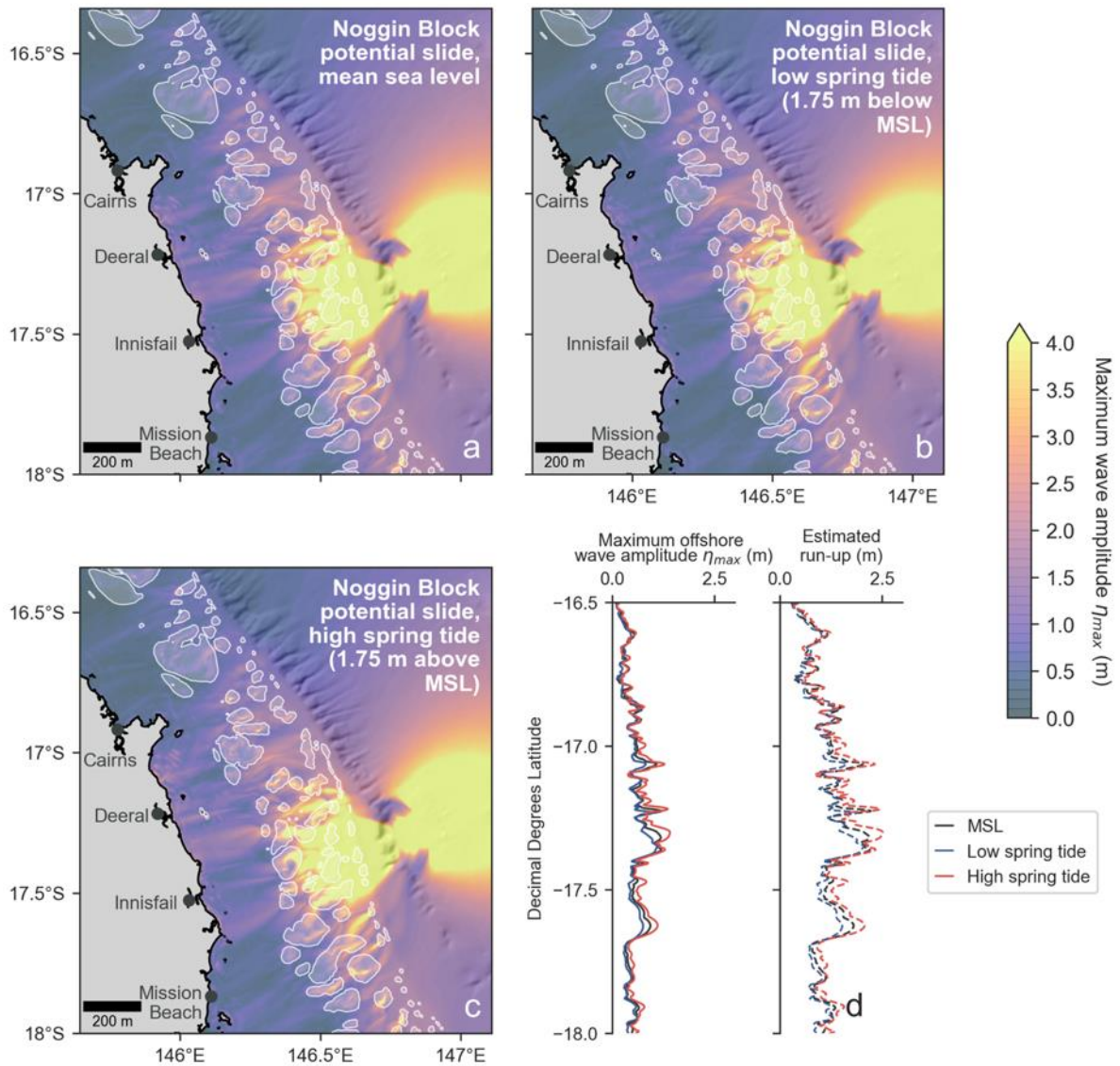


672

673 **Figure 14.** Maximum wave amplitude distributions for the hypothetical M_w 8.5 Solomon Islands earthquake
674 scenario simulated at a) mean sea level (MSL, bottom friction coefficient $C_D=0.1522$ on platforms, shown in
675 white) b) low spring tide (1.75 m below MSL, $C_D=0.1522$ on platforms), and c) high spring tide (1.75 m above
676 MSL, $C_D=0.1522$ on platforms). d) Corresponding maximum offshore wave amplitude and estimated run-up
677 distributions. Maximum run-up estimates are 26 cm for the MSL scenario, 25 cm for the low spring tide scenario,
678 and 26 cm for the high spring tide scenario. Offshore wave amplitudes were interpolated along the 25 m isobath.

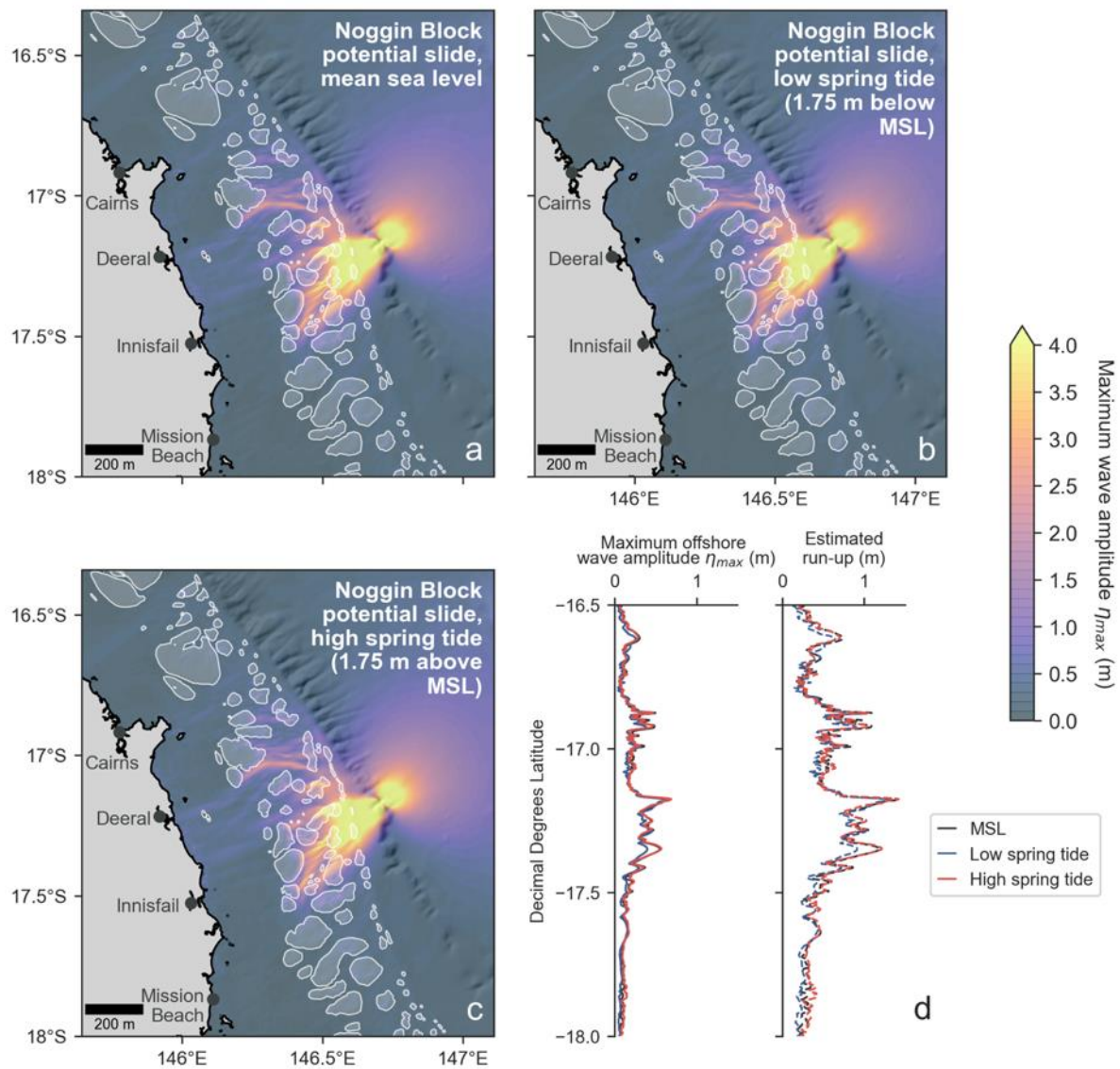
679

680



681

682 **Figure 15.** Maximum wave amplitude distributions for the Gloria Knolls Slide scenario simulated at a) mean sea
 683 level (bottom friction coefficient $C_D=0.1522$ on platforms, shown in white) b) low spring tide (1.75 m below
 684 MSL, $C_D=0.1522$ on platforms), and c) high spring tide (1.75 m above MSL, $C_D=0.1522$ on platforms). d)
 685 Corresponding maximum offshore wave amplitude and estimated run-up distributions. Maximum run-up
 686 estimates are 1.4 m for the MSL scenario, 1.4 m for the low spring tide scenario, and 1.3 m for the high spring
 687 tide scenario. Offshore wave amplitudes were interpolated along the 25 m isobath.



688

689 **Figure 16.** Maximum wave amplitude distributions for the Noggin Block potential slide scenario simulated at a)
 690 mean sea level (bottom friction coefficient $C_D=0.1522$ on platforms, shown in white) b) low spring tide (1.75 m
 691 below MSL, $C_D=0.1522$ on platforms), and c) high spring tide (1.75 m above MSL, $C_D=0.1522$ on platforms). d)
 692 Corresponding maximum offshore wave amplitude and estimated run-up distributions. Maximum run-up
 693 estimates are 1.4 m for the MSL scenario, 1.4 m for the low spring tide scenario, and 1.3 m for the high spring
 694 tide scenario. Offshore wave amplitudes were interpolated along the 25 m isobath.

695

696 5. Discussion

697

698 5.1. The impact of the GBR's ecosystem-scale complexity on tsunami propagation

699 Our results show that tsunamis are strongly impacted by the presence of coral cover in the

700 GBR. Across many of the “coral-covered platforms” simulations, maps showing maximum

701 wave amplitude distributions show clear “shadow zones” landward of reef platforms, where

702 amplitudes markedly decrease. These impacts are especially pronounced for the Mw 9.0
703 Solomon Islands earthquake scenario (Figure 9), the Gloria Knolls submarine landslide
704 scenario (Figure 11) and the Noggin Block potential submarine landslide scenario (Figure 12).
705 These declines in wave amplitude are driven by elevated frictional dissipation over coral-
706 covered reef platforms. We eliminate the possibility that wave breaking contributed to energy
707 dissipation, as wave-breaking was not detected in any of the simulations due to the tsunamis'
708 large wavelengths in comparison to their amplitudes. These results reaffirm the prevailing
709 notion that the GBR acts as a regional buffer to tsunamis (Baba et al. 2008; Wei et al. 2015;
710 Xing et al. 2015; Webster et al. 2016; Puga-Bernabéu et al. 2019). They are also consistent
711 with previous findings from other modelling studies, especially those that include wider reef
712 platforms in their assessments (Kunkel et al. 2006; Gelfenbaum et al. 2011; Yao et al. 2012),
713 which allows the cumulative impact of frictional dissipation to dominate. Therefore, we
714 propose that the effect of live coral cover should be directly incorporated into future hazard
715 assessments of the northeastern Australian margin, as we anticipate it will have a detrimental
716 impact on propagating tsunamis.

717
718 The energy-diminishing impact of coral cover becomes most apparent when comparing the
719 “coral-covered platforms” simulations with the “smooth platforms” simulations. When coral
720 cover is removed, amplitudes increase across each source scenario tested here. Notably, run-
721 up projections increase as much as 24% for the Mw 9.0 earthquake source (Figure 10), and they
722 exhibit a maximum of a nearly four-fold change for the Noggin Block potential slide (Figure
723 13). These increases in amplitude and run-up imply that while coral cover in the GBR may
724 currently have a buffering effect on tsunami wave energy, this effect may diminish as reef
725 ecosystems in the GBR continue to decline under the physiological stressors (e.g., heat stress,
726 acidity stress) that accompany anthropogenic climate change (Hughes et al. 2018). Generally

727 speaking, the structural complexity of coral reefs is expected to deteriorate as reef-building
728 species are lost and as ecosystems transition to algal-dominated states (Bellwood et al. 2004;
729 Alvarez-Filip et al. 2009; Wild et al. 2011). This deterioration of structural complexity is
730 expected to lessen frictional dissipation of wind wave energy (Harris et al. 2018; de Lalouvière
731 et al. 2020). Based on our results, we expect a similar outlook for tsunami wave hazards. This
732 loss of buffering capacity may be further compounded by the effects of sea level rise, where
733 some assessments have forecasted heightened tsunami hazard under current projections (Li et
734 al. 2018; Nagai et al. 2020).

735

736 Across source scenarios, there are prominent discrepancies in the magnitude of the amplitude
737 and run-up increases when coral cover is removed. For instance, while the M_w 8.0 earthquake
738 scenario experiences marginal increases (4% maximum, see Figure 10), M_w 9.0 scenario
739 experiences substantial jumps in offshore amplitude (up to 31%) when platforms are smoothed.
740 This implies that the degree of coral-induced frictional dissipation at bed is different across
741 source scenarios. Our findings demonstrate that these differences in frictional dissipation are
742 directly related to wave amplitude (and thus, wave energy). Particle velocity (note: this is
743 different to wave *celerity*) is a function of wave amplitude (Nielsen 1992), and therefore, waves
744 of differing amplitudes experience different degrees of dissipation due to shear stress at bed.
745 This amplitude-mediated discrepancy in particle velocity is best exemplified by comparing
746 earthquake scenarios, where tsunami amplitude was altered by changing the magnitude and
747 slip displacement of the initial coseismic source (Figure 4, see Table 1 for source parameters).
748 For the M_w 8.0 Solomon Islands earthquake scenario, bed particle velocities are relatively low
749 (< 1 cm/s) throughout the computational domain given the relatively low tsunami amplitudes
750 produced by the source. However, for the M_w 8.5 and M_w 9.0 earthquake scenarios, particle
751 velocities are much higher on the shelf (> 5 cm/s). Moreover, in their corresponding “smooth

752 platforms” simulations, particle velocities are more elevated atop the reef platforms than in the
753 “coral-covered platforms” simulations, which further reflects the dissipative effect of coral
754 cover. As wave energy dissipation through shear stress is proportional to the square of the
755 particle velocity (see Eq. 1), the higher velocities computed for higher-magnitude earthquake
756 tsunamis result in greater overall wave energy dissipation via bottom friction when coral cover
757 is present. This also explains why a relatively large degree of attenuation is observed for the
758 landslide-generated tsunamis, both of which produce similarly high waves (9 m and 3.5 m for
759 the landward-propagating waves, respectively). Our results show that tsunami amplitude,
760 which ultimately depends on the magnitude and proximity of the triggering source, should also
761 be considered when examining the buffering capacity of natural defences such as coral reefs.

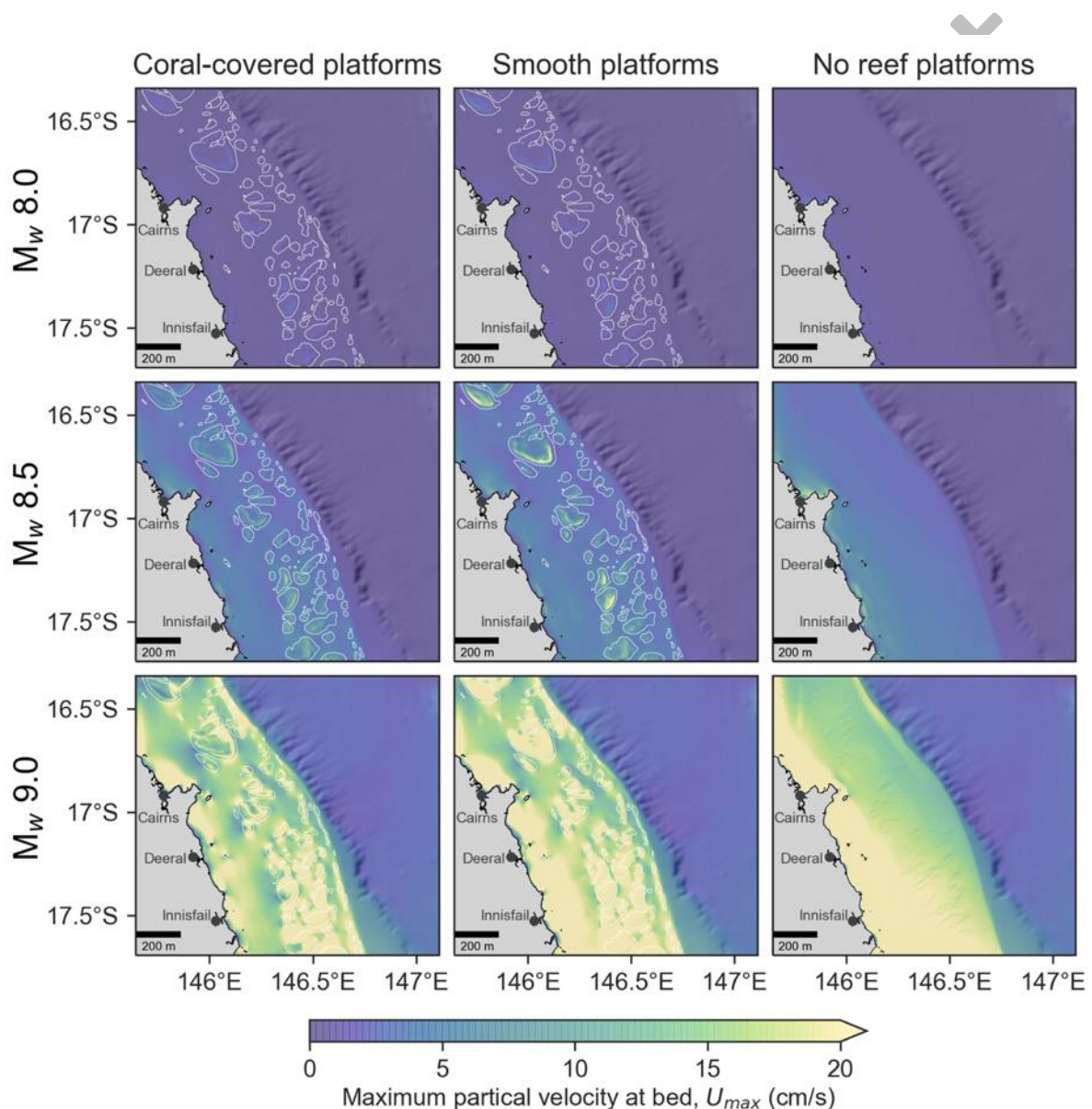
762

763 While the GBR generally acts as a buffer to tsunami wave energy, despite its namesake, the
764 GBR itself does not form a continuous barrier on the mid- to outer shelf, especially in the
765 central region (Figure 3). As a result, the buffering effect offered by coral cover varies
766 considerably alongshore. Turning again to the Solomon Islands earthquake scenarios (Figure
767 10), when coral cover is removed, the largest increases in wave amplitude and run-up tend to
768 occur landward of broad reef platforms (see also Figure 9a, b). On the other hand, areas that
769 lie between inter-reef passages, or gaps, exhibit smaller increases in amplitude and run-up. This
770 phenomenon is consistent across source scenarios, and it is particularly pronounced in cases
771 where tsunami amplitudes are relatively high. This implies that the protectiveness offered by
772 coral cover varies alongshore because of platform placement; if coral-covered platforms
773 (particularly broad platforms) are positioned between the incoming tsunami and the shoreline,
774 they are more inclined to dampen the tsunami.

775

776 To summarise, reef cover contributes substantially to the overall buffering capacity of the
 777 GBR, which is consistent with previous findings (e.g., Kunkel et al. 2006). However, the
 778 GBR’s buffering capacity for any given location alongshore depends on various site-specific
 779 factors, including the presence of coral cover, the relative positioning of the platforms, and
 780 tsunami amplitude.

781



782 **Figure 17.** Maximum bed particle velocities (in cm/s) across the computational domain for each the M_w 8.0
 783 Solomon Islands earthquake scenario (top row), the M_w 8.5 scenario (middle row), and the M_w 9.0 scenario
 784 (bottom row). Columns are aligned based on their corresponding “coral-covered platforms” simulations (left
 785 column), “smooth platforms” simulations (middle column), and “no reef platforms” simulations (right column).

787

788

789 5.2. The impact of the GBR's bathymetric-scale complexity on tsunami propagation
790 Our simulations reveal the remarkably complex ways in which tsunami waves interact with the
791 larger-scale bathymetric features (i.e., platforms, shoals, etc.) that comprise the GBR. Of
792 particular note is the platforms' ability to focus tsunami wave energy towards shore (see Figure
793 8 and Online Resource 3 for the M_w 8.5 Solomon Islands earthquake simulations). In a manner
794 analogous to a convex lens focussing light, platforms cause the incoming tsunami waves to
795 refract inwards towards their shallower depths, inciting shoaling, positive wave interference,
796 and subsequent heightening of wave trains. Shoaling and heightening of tsunami waves over
797 shallow reefs has been observed by others, both from field-based and modelling evidence
798 (Chatenoux and Peduzzi 2005; Gelfenbaum et al. 2011). Interestingly, frictional dissipation by
799 coral cover appears to fully or partially counteract these focussing effects, where waves
800 subsequently dampen after growing in amplitude over the platforms (e.g., Figure 9).
801 Consequently, smoothing the domain tends to enhance the platforms' ability to focus wave
802 energy. This is demonstrated by the higher-amplitude, landward wave trains shown in wave
803 amplitude distributions (e.g., Figure 9). Some platforms appear to more effectively focus wave
804 energy than others, and we suspect this is due to factors such as reef morphology, size, and
805 submergence depth. A more systematic investigation of platform characteristics warranted to
806 test this hypothesis, particularly as coral reef cover is expected to decline in the future.

807

808 In addition to focussing effects, simulated tsunamis exhibit a complex interplay of additional
809 behaviours when interacting with platforms, such as diffraction, reflection, and scattering of
810 wave trains (see Online Resource 5 for example). These effects are most pronounced for the
811 landslide-generated tsunami cases (see Section 4.4), and we tentatively suggest that this is due
812 to their shorter wavelengths. Our simulations further reinforce the important role that local
813 bathymetry plays in modulating tsunami behaviour, particularly in shallow reef environments

814 (Baba et al. 2008; Dilmen et al. 2018). This potent, complex, and site-specific control on
815 tsunami propagation further underscores the need to evaluate tsunami hazard on a case-by-case
816 basis.

817

818 We also highlight the intriguing role of inter-reef passages, or gaps, in modulating tsunami
819 behaviour as it crosses the shelf. Many have hypothesized that gaps in the reef structure worsen
820 the tsunami hazard, as the gaps act as low-resistance conduits that amplify wave energy (Nott
821 1997; Liu et al. 2005; Gelfenbaum et al. 2011; McAdoo et al. 2011; Roger et al. 2014). In our
822 simulations, porous gaps in the reef structure certainly permit wave energy to pass through to
823 the coastline. However, there is little evidence to support the notion that the gaps amplify
824 waves. In fact, due to focussing, amplification of wave amplitudes occurs *over* the platforms
825 rather than *between* them (e.g., Figure 9, Figure 11). In the case of the GBR, many of the
826 platforms appear to be wide enough, deep enough, far enough apart, and far enough from the
827 coastline such that the inter-reef gaps do not pose a significant hazard. This is in contrast to
828 many fringing reef systems, where gaps can be quite narrow, shallow, and close to shore. We
829 therefore suggest that for the GBR, the wave focussing ability of platforms may be of greater
830 concern for the northeastern Australian coastline than the presence of gaps in the reef structure.

831

832 Overall, the GBR's underlying bathymetric structure contributes significantly to its buffering
833 capacity, and this becomes apparent when platforms are removed from simulations (see Figure
834 10 and Figure 13). When platforms are removed, waves are permitted to propagate smoothly
835 and uninterrupted across the shelf, highlighting the highly obstructive nature of the platforms
836 themselves. Offshore wave amplitudes and run-up distributions increase alongshore across all
837 source scenarios when platforms are removed. These findings are consistent with previous
838 work which suggests that bathymetric irregularities on the shelf exert large control on the

839 eventual run-up distribution at the coast (Baba et al. 2008; Schambach et al. 2018). Even as the
840 GBR is interrupted by gaps, the presence reef structure appears to provide at least some benefit
841 to nearly all areas of the coastline examined in this study.

842

843 5.3. Broader implications surrounding the GBR's impact on tsunami hazard

844 This study has revealed wider implications for communities situated along the northeastern
845 Australian coastline. Firstly, from a mitigation perspective, the GBR may offer greater
846 protection for more severe tsunami events. In particular, the GBR may offer natural protection
847 against near-field landslide sources, which are notoriously difficult to predict and forecast
848 (Tappin et al. 1999; Harbitz et al. 2014). While this may take some pressure off warning
849 systems, we stress that coastal communities should not rely upon the GBR alone to reduce their
850 vulnerability to tsunami hazards. A holistic strategy for tsunami hazard preparedness ultimately
851 should include risk awareness, hazard education, resilient infrastructure, and robust early
852 warning systems (Baird et al. 2005; Liu et al. 2005; Dominey-Howes et al. 2007; Mori et al.
853 2011).

854

855 Secondly, from a *future* mitigation perspective, our work suggests that the declining coral
856 health, which is associated with globally-mediated anthropogenic climate change (De'ath et al.
857 2012; Hughes et al. 2018), will have an overall adverse effect on the GBR's defensive
858 capability. In this context, today's reef-buffering asset may be tomorrow's liability. Areas of
859 shoreline that are best-protected by broad, expansive coral-covered platforms may experience
860 the highest inundation risk in the future as coral die-off continues and as architectural
861 complexity deteriorates (Alvarez-Filip et al. 2009), enhancing the platforms' ability to focus
862 energy towards shore rather than attenuating it. These local differences reinforce the need for

863 site-specific hazard assessments when considering tsunami hazard on the northeastern
864 Australian margin in the future.

865

866 5.4. Reconciling differing interpretations of coral reef impact on tsunamis

867 In light of our results, we address some of the contrasting interpretations in the literature around
868 the impact of coral reefs on tsunami hazard. Firstly, while the GBR, being an offshore barrier
869 system, buffers the tsunami hazard for the more distant Australian coastline, other reef
870 environments (in particular, narrow fringing reefs that surround populated inner islands) could
871 exacerbate tsunami hazard through behaviours such as shoaling, focussing, and bore formation
872 (Chatenoux and Peduzzi 2005; Fritz et al. 2011; Gelfenbaum et al. 2011; Yao et al. 2012).
873 Indeed, our simulations showcase shoaling and focussing on platforms, which locally augment
874 wave amplitudes at the intra-platform scale. A more rigorous inundation study would be needed
875 to confirm whether this translates to increased hazard within the lagoons, shoals, and islands
876 that rest within the platforms. Therefore, coral reefs could have either beneficial or detrimental
877 effects on the overall hazard depending on the type reef system in question and the proximity
878 of coastal communities and assets to the site of the most severe shoaling/focussing. In the
879 debate surrounding reef protectiveness against tsunamis, a distinction must be made between
880 fringing reef systems and offshore barrier systems, as they have different implications for
881 proximity to wave focussing effects, and therefore, exposure.

882

883 On the other hand, we also note potential ambiguities around the ways in which the impact of
884 coral reefs is reported in post-tsunami field surveys. From our simulations and others (Kunkel
885 et al. 2006; Uslu et al. 2010; Gelfenbaum et al. 2011), there is evidently a strong theoretical
886 basis to support the fact that coral reefs can dissipate tsunami wave energy, reducing the
887 tsunami *hazard*. However, this overall reduction in hazard may not be sufficient to completely

888 reduce the *physical vulnerability* and *exposure* of coastal communities (Uslu et al. 2010). When
889 discussing the buffering role of reefs, many have highlighted that despite being within close
890 proximity to reefs, coastal assets have nonetheless been destroyed during tsunami events (e.g.,
891 Baird et al. 2005), leading some to conclude that coral reefs provide no protective benefit to
892 coastal communities. In these cases, the reefs could very well have buffered the overall tsunami
893 hazard, reducing the overall inundation and run-up extent. However, this protective benefit
894 may not have been sufficient to completely shield coastal communities that were situated close
895 to shore. Care must be taken when retrospectively interpreting the role that coral reefs may
896 have played in reducing tsunami hazard along a shoreline, and a clear distinction should be
897 made between *hazard reduction* and *risk reduction*, which lies at the intersection between
898 hazard, exposure, and vulnerability.

899

900 5.5. Study limitations and future work

901 Uncertainties persist that could complicate such future tsunami hazards assessments in coral
902 reef environments. Firstly, at the ecosystem-scale, the relationship between coral rugosity and
903 community composition requires more precise quantification on an intra-reef platform scale
904 (Rogers et al. 2016). This will continue to be a pressing task in the future, as profound
905 ecological shifts may be precipitated by both the immediate aftermath of the tsunami impact
906 and longer-term environmental changes, thus affecting ecosystem-scale structural complexity
907 (Madin and Connolly 2006; Alvarez-Filip et al. 2009; Ferrari et al. 2016; Hughes et al. 2018).
908 While platform degradation and bioerosion is largely anticipated to flatten coral reefs (Alvarez-
909 Filip et al. 2009), the shorter-term impact of these and other stressors on ecosystem-scale
910 rugosity is still not precisely known. These ecosystems should be stringently monitored to
911 better assess how coastal hazard severity as a whole will be transformed in these areas.
912 Additionally, the approach used to parameterize bottom shear stress, though very common both

913 in the field and in modelling studies, may need to be reconfigured to account for more complex
914 tsunami interactions and subgrid turbulent dissipation within the 3D reef structure (Lowe et al.
915 2008; Kim et al. 2009; Rosman and Hench 2011). Moreover, these more complex interactions
916 may be better represented by a Navier Stokes model rather than a depth-averaged wave model
917 (Kazolea et al. 2019).

918

919 On a larger scale, it is worth exploring the potential impact of undular bores that could arise
920 and break on the platforms themselves, as they could play an additional role in dissipating wave
921 energy offshore (Grilli et al. 2012; Glimsdal et al. 2013). These wave features would not have
922 been resolved in our coarser-resolution runs (Schambach et al. 2018), as capturing them
923 quickly becomes very demanding computationally (<10 m resolution required, Grilli et al.
924 2012). Also, while our study emphasizes the effect of the GBR on offshore amplitudes and
925 projected run-up distributions, ultimately, tsunami-induced surges and bores deliver the force
926 and high water levels that cause destruction to coastal communities onshore (Koshimura et al.
927 2009; Nistor et al. 2009; Nouri et al. 2010). Further work is warranted to establish whether the
928 reduction in offshore wave amplitude translates to a reduced hazard onshore, and this would
929 necessitate the deployment of higher-resolution inundation simulations.

930

931 Finally, our study was not designed to provide a reappraised, comprehensive hazard assessment
932 for the northeastern Australian coastline although our findings suggest that the reef's role
933 should be considered in future assessments. That being said, we stress the need for a robust
934 parameterization of reef roughness (Nelson 1996; Rosman and Hench 2011). Furthermore, as
935 indicated by sensitivity analyses (see Online Resource 2), these propagation simulations
936 require high spatial resolution (200 m for earthquake sources and 100 m or less for landslide
937 sources) in order to properly capture the reef structure and to resolve complex tsunami-reef

938 interactions. While this increases computational demand, we nonetheless deem it worthwhile
939 to consider the role of the reef, as current assessments may be over-estimating tsunami risk in
940 northeast Australia. Additionally, a more meaningful assessment of the submarine landslide
941 tsunami hazard is needed to better understand the timing, frequency, and magnitude of these
942 events. In the future, it may be worth considering more complex failure dynamics (i.e. landslide
943 deformation and two-way coupling with the water column), which could alter the run-up results
944 (Masson et al. 2006; Geist et al. 2009; Abadie et al. 2010), but we anticipate that accounting
945 for these dynamics will not alter the overall conclusions established here about the buffering
946 effect of the GBR. Addressing these limitations will enable more reliable forecasting as the
947 fate of the world's coral reefs becomes clearer with time.

948

949 6. Conclusions

950 This study demonstrates the nuanced interactions between tsunamis and coral reef systems. In
951 agreement with previous work we find that the Great Barrier Reef (GBR), both in terms of
952 coral cover and larger-scale bathymetric complexity, acts as a large-scale regional buffer
953 against tsunamis. However, the reef appears to provide greater protection against higher-
954 amplitude tsunamis due to the larger computed particle velocities at bed, which directly dictates
955 the degree of frictional dissipation through shear stress. Additionally, we find that the
956 protectiveness offered by the GBR locally depends on coral cover and platform distribution.
957 We also find that wave focussing by reef platforms could pose a greater hazard than the gaps
958 between platforms, which have been previously thought to amplify waves. In the context of
959 the larger debate about whether coral reefs reduce tsunami hazards for coastal communities,
960 we conclude that differing interpretations can be reconciled when considering site-specific
961 factors.

962

963

964

Acknowledgements

965

966 We extend our sincere gratitude to Fengyan Shi for his assistance with model set-up and

967 troubleshooting. We also thank Lorena Moscardelli for allowing us to reproduce a significant

968 portion of her submarine landslide database for this work. We are grateful to Tristan Salles,

969 Jon Hill, and Greg Houseman for their constructive and insightful comments. Stewart Allen

970 and Diana Greensdale from the Australian Bureau of Meteorology provided earthquake source

971 parameters. Computational resources were provided by the National Computational

972 Infrastructure (NCI) in Canberra, Australia, which is supported by the Australian

973 Commonwealth Government. We also thank the Sydney Informatics Hub at the University of

974 Sydney for the provisioning of both expertise and computing power by their high-performance

975 computing facility (Artemis).

976

977

References

978

979
980 Abadie S, Morichon D, Grilli S, Glockner S (2010) Numerical simulation of waves generated
981 by landslides using a multiple-fluid Navier–Stokes model. *Coast Eng* 57:779–794.

982 <https://doi.org/10.1016/j.coastaleng.2010.03.003>

983 Aksu AE, Hiscott RN (1992) Shingled Quaternary debris flow lenses on the north-east
984 Newfoundland Slope. *Sedimentology* 39:193–206. [https://doi.org/10.1111/j.1365-](https://doi.org/10.1111/j.1365-3091.1992.tb01034.x)

985 [3091.1992.tb01034.x](https://doi.org/10.1111/j.1365-3091.1992.tb01034.x)

986 Alfaro E, Holz M (2014) Seismic geomorphological analysis of deepwater gravity-driven
987 deposits on a slope system of the southern Colombian Caribbean margin. *Mar Pet Geol*
988 57:294–311. <https://doi.org/10.1016/j.marpetgeo.2014.06.002>

989 Alvarez-Filip L, Dulvy NK, Gill JA, et al (2009) Flattening of Caribbean coral reefs: region-
990 wide declines in architectural complexity. *Proc R Soc B Biol Sci* 276:3019–3025.

991 <https://doi.org/10.1098/rspb.2009.0339>

992 Alves TM, Cartwright JA (2009) Volume balance of a submarine landslide in the Espírito
993 Santo Basin, offshore Brazil: quantifying seafloor erosion, sediment accumulation and
994 depletion. *Earth Planet Sci Lett* 288:572–580. <https://doi.org/10.1016/j.epsl.2009.10.020>

995 Amante C, Eakins BW (2009) ETOPO1 Arc-Minute Global Relief Model: Procedures, Data
996 Sources and Analysis. NOAA Technical Memorandum NESDIS NGDC-24. National
997 Geophysical Data Center, NOAA

998 Andrews JC, Bode L (1988) The tides of the central Great Barrier Reef. *Cont Shelf Res*

999 8:1057–1085. [https://doi.org/10.1016/0278-4343\(88\)90039-8](https://doi.org/10.1016/0278-4343(88)90039-8)

1000 Ashabranner LB, Tripsanas EK, Shipp RC (2010) Multi-direction Flow in a Mass-Transport
1001 Deposit, Santos Basin, Offshore Brazil. In: Mosher DC, Shipp RC, Moscardelli L, et al.
1002 (eds) Submarine Mass Movements and Their Consequences. Springer Netherlands,
1003 Dordrecht, pp 247–255

1004 Australian Bureau of Meteorology (2020) Past Tsunami Events.
1005 <http://www.bom.gov.au/tsunami/history/index.shtml>

1006 Baba T, Mleczek R, Burbidge D, et al (2008) The effect of the great barrier reef on the
1007 propagation of the 2007 Solomon Islands tsunami recorded in Northeastern Australia.
1008 *Pure Appl Geophys* 165:2003–2018. <https://doi.org/10.1007/s00024-008-0418-5>

1009 Baird AH, Campbell SJ, Anggoro AW, et al (2005) Acehnese Reefs in the Wake of the Asian
1010 Tsunami Centre for Coral Reef Biodiversity. *Curr Biol* 15:1926–1930.
1011 <https://doi.org/10.1016/j.cub.2005.09.036>

1012 Barnes PM, Lewis KB (1991) Sheet slides and rotational failures on a convergent margin: the
1013 Kidnappers Slide, New Zealand. *Sedimentology* 38:205–221.
1014 <https://doi.org/10.1111/j.1365-3091.1991.tb01257.x>

1015 Beaman RJ (2010) Project 3D-GBR: A high-resolution depth model for the Great Barrier
1016 Reef and Coral Sea. Project 2.5i.1a Final Report, Marine and Tropical Sciences
1017 Research Facility, Cairns, Australia

1018 Behrmann JH, Völker D, Geersen J, et al (2014) Size-Frequency Relationship of Submarine
1019 Landslides at Convergent Plate Margins: Implications for Hazard and Risk Assessment.
1020 In: Krastel S, Behrmann J-H, Völker D, et al. (eds) Submarine Mass Movements and
1021 Their Consequences: 6th International Symposium. Springer International Publishing,
1022 Cham, pp 165–175

1023 Bellwood DR, Hughes TP, Folke C, Nyström M (2004) Confronting the coral reef crisis.
1024 *Nature* 429:827–833. <https://doi.org/10.1038/nature02691>

1025 Boudon G, Le Friant A, Komorowski J, et al (2007) Volcano flank instability in the Lesser
1026 Antilles Arc: diversity of scale, processes, and temporal recurrence. *J Geophys Res*
1027 *Solid Earth* 112:B08205. <https://doi.org/10.1029/2006JB004674>

1028 Bourget J, Zaragosi S, Rodriguez M, et al (2013) Late Quaternary megaturbidites of the Indus
1029 Fan: Origin and stratigraphic significance. *Mar Geol* 336:10–23.
1030 <https://doi.org/10.1016/j.margeo.2012.11.011>

1031 Bourget J, Zaragosi S, Ellouz-Zimmermann N, et al (2011) Turbidite system architecture and
1032 sedimentary processes along topographically complex slopes: the Makran convergent
1033 margin. *Sedimentology* 58:376–406. <https://doi.org/10.1111/j.1365-3091.2010.01168.x>

1034 Boyd R, Keene J, Hubble T, et al (2010) Southeast Australia: A Cenozoic Continental
1035 Margin Dominated by Mass Transport. In: Submarine Mass Movements and Their
1036 Consequences. pp 491–502

1037 Bozec Y-M, Alvarez-Filip L, Mumby PJ (2015) The dynamics of architectural complexity on
1038 coral reefs under climate change. *Glob Chang Biol* 21:223–235.
1039 <https://doi.org/10.1111/gcb.12698>

1040 Brune S, Babeyko a. Y, Ladage S, Sobolev S V. (2010) Landslide tsunami hazard in the
1041 Indonesian Sunda Arc. *Nat Hazards Earth Syst Sci* 10:589–604.
1042 <https://doi.org/10.5194/nhess-10-589-2010>

1043 Burke L, Reytar K, Spalding M, Perry A (2011) Reefs at risk revisited. World Resources
1044 Institute, Washington, DC

1045 Calvès G, Huuse M, Clift PD, Brusset S (2015) Giant fossil mass wasting off the coast of
1046 West India: The Nataraja submarine slide. *Earth Planet Sci Lett* 432:265–272.
1047 <https://doi.org/10.1016/j.epsl.2015.10.022>

- 1048 Camerlenghi A, Accettella D, Costa S, et al (2009) Morphogenesis of the SW Balearic
1049 continental slope and adjacent abyssal plain, Western Mediterranean Sea. *Int J Earth Sci*
1050 98:735. <https://doi.org/10.1007/s00531-008-0354-8>
- 1051 Campbell DC, Mosher DC (2010) Middle to Late Miocene Slope Failure and the Generation
1052 of a Regional Unconformity Beneath the Western Scotian Slope, Eastern Canada BT -
1053 Submarine Mass Movements and Their Consequences. In: Mosher DC, Shipp RC,
1054 Moscardelli L, et al. (eds). Springer Netherlands, Dordrecht, pp 645–655
- 1055 Canals M, Lastras G, Urgeles R, et al (2004) Slope failure dynamics and impacts from
1056 seafloor and shallow sub-seafloor geophysical data: case studies from the COSTA
1057 project. *Mar Geol* 213:9–72. <https://doi.org/10.1016/j.margeo.2004.10.001>
- 1058 Carlson PR, Karl HA, Edwards BD, et al (1993) Mass movement related to large submarine
1059 canyons along the Beringian Margin, Alaska. In: *Submarine Landslides: Selected*
1060 *Studies in the US Exclusive Economic Zone*. U.S. Geological Survey Bulletin,
1061 Washington, DC, p 104
- 1062 Center for International Earth Science Information Network (CIESIN) (2018) Gridded
1063 Population of the World, Version 4 (GPWv4): Population Density Adjusted to Match
1064 2015 Revision UN WPP Country Totals, Revision 11. NASA Socioeconomic Data and
1065 Applications Center (SEDAC), Columbia University, Palisades, NY
- 1066 Chatenoux B, Peduzzi P (2005) Analysis on the Role of Bathymetry and other Environmental
1067 Parameters in the Impacts from the 2004 Indian Ocean Tsunami. UNEP/GRID-Europe,
1068 Geneva
- 1069 Chatenoux B, Peduzzi P (2007) Impacts from the 2004 Indian Ocean Tsunami: Analysing the
1070 potential protecting role of environmental features. *Nat Hazards* 40:289–304.
1071 <https://doi.org/10.1007/s11069-006-0015-9>
- 1072 Chaytor JD, Twichell DC, Lynett P, Geist EL (2010) Distribution and Tsunamigenic
1073 Potential of Submarine Landslides in the Gulf of Mexico. In: Mosher DC, Shipp RC,
1074 Moscardelli L, et al. (eds) *Submarine Mass Movements and Their Consequences*.
1075 Springer Netherlands, Dordrecht, pp 745–754
- 1076 Chaytor JD, Geist EL, Paull CK, et al (2016) Source Characterization and Tsunami Modeling
1077 of Submarine Landslides Along the Yucatán Shelf/Campeche Escarpment, Southern
1078 Gulf of Mexico. *Pure Appl Geophys* 173:4101–4116. [https://doi.org/10.1007/s00024-](https://doi.org/10.1007/s00024-016-1363-3)
1079 [016-1363-3](https://doi.org/10.1007/s00024-016-1363-3)
- 1080 Chaytor JD, ten Brink US, Solow AR, Andrews BD (2009) Size distribution of submarine
1081 landslides along the U.S. Atlantic margin. *Mar Geol* 264:16–27.
1082 <https://doi.org/10.1016/j.margeo.2008.08.007>
- 1083 Chaytor JD, Twichell DC, ten Brink US (2012) A Reevaluation of the Munson-Nygren-
1084 Retriever Submarine Landslide Complex, Georges Bank Lower Slope, Western North
1085 Atlantic. In: Yamada Y, Kawamura K, Ikehara K, et al. (eds) *Submarine Mass*
1086 *Movements and Their Consequences*. Springer Netherlands, Dordrecht, pp 135–146
- 1087 Collot J, Lewis K, Lamarche G, Lallemand S (2001) The giant Ruatoria debris avalanche on
1088 the northern Hikurangi margin, New Zealand: Result of oblique seamount subduction. *J*
1089 *Geophys Res Solid Earth* 106:19271–19297. <https://doi.org/10.1029/2001JB900004>
- 1090 Dalla Valle G, Gamberi F, Foglini F, Trincardi F (2015) The Gondola Slide: A mass
1091 transport complex controlled by margin topography (South-Western Adriatic Margin,
1092 Mediterranean Sea). *Mar Geol* 366:97–113.
1093 <https://doi.org/10.1016/j.margeo.2015.05.001>
- 1094 Davies G, Griffin J (2018) The 2018 Australian Probabilistic Tsunami Hazard Assessment:
1095 Hazard from Earthquake Generated Tsunamis. Geoscience Australia, Canberra
- 1096 Davies PJ, McKenzie JA, Palmer-Julson AA, et al (1991) Site 819. In: McKenzie JA,
1097 Palmer-Julson AA, Betzler C, et al. (eds) *Proceedings of the Ocean Drilling Program*,

1098 Part A: Initial Reports. College Station: TX (Ocean Drilling Program), p 451

1099 De'ath G, Fabricius KE, Sweatman H, Puotinen M (2012) The 27-year decline of coral cover
1100 on the Great Barrier Reef and its causes. *Proc Natl Acad Sci U S A* 109:17995–17999.
1101 <https://doi.org/10.1073/pnas.1208909109>

1102 Dillon WP, Risch JS, Scanlon KM, et al (1993) Ancient crustal fractures control the location
1103 and size of collapsed blocks at the Blake Escarpment, east of Florida. In: Schwab W,
1104 Lee H, Twichell D (eds) *Submarine landslides: Selected Studies in the US Exclusive
1105 Economic Zone*. US Geological Survey Bulletin, pp 54–59

1106 de Lalouvière C la H, Gracia V, Sierra JP, et al (2020) Impact of Climate Change on
1107 Nearshore Waves at a Beach Protected by a Barrier Reef. *Water* 12:1681

1108 Dilmen DI, Roe GH, Wei Y, Titov V V (2018) The Role of Near-Shore Bathymetry During
1109 Tsunami Inundation in a Reef Island Setting: A Case Study of Tutuila Island. *Pure Appl
1110 Geophys* 175:1239–1256. <https://doi.org/10.1007/s00024-018-1769-1>

1111 Dingle R V (1980) Large allochthonous sediment masses and their role in the construction of
1112 the continental slope and rise off southwestern Africa. *Mar Geol* 37:333–354.
1113 [https://doi.org/10.1016/0025-3227\(80\)90109-7](https://doi.org/10.1016/0025-3227(80)90109-7)

1114 Dingle R V (1977) The anatomy of a large submarine slump on a sheared continental margin
1115 (SE Africa). *J Geol Soc London* 134:293–310. <https://doi.org/10.1144/gsjgs.134.3.0293>

1116 Dominey-Howes D (2007) Geological and historical records of tsunami in Australia. *Mar
1117 Geol* 239:99–123. <https://doi.org/10.1016/j.margeo.2007.01.010>

1118 Dominey-Howes D, Papatoma-Köhle M, Bird D, et al (2007) Letter to the Editor: the
1119 Australian Tsunami Warning System and lessons from the 2 April 2007 Solomon
1120 Islands tsunami alert in Australia. *Nat Hazards Earth Syst Sci* 7:571–572

1121 Droz L, Dos Reis AT, Rabineau M, et al (2006) Quaternary turbidite systems on the northern
1122 margins of the Balearic Basin (Western Mediterranean): a synthesis. *Geo-Marine Lett*
1123 26:347–359

1124 Eichhubl P, Greene HG, Maher N (2002) Physiography of an active transpressive margin
1125 basin: high-resolution bathymetry of the Santa Barbara basin, Southern California
1126 continental borderland. *Mar Geol* 184:95–120. [https://doi.org/10.1016/S0025-3227\(01\)00280-8](https://doi.org/10.1016/S0025-3227(01)00280-8)

1127 Elger J, Berndt C, Krastel S, et al (2015) The Fram Slide off Svalbard: a submarine landslide
1128 on a low-sedimentation-rate glacial continental margin. *J Geol Soc London* 172:153–
1129 156. <https://doi.org/10.1144/jgs2014-055>

1131 Elmore RD, Pilkey OH, Clearly WJ, Curran HA (1979) Black Shell turbidite, Hatteras
1132 Abyssal Plain, western Atlantic Ocean. *Geol Soc Am Bull* 90:1165–1176.
1133 [https://doi.org/10.1130/0016-7606\(1979\)90<1165:BSTHAP>2.0.CO;2](https://doi.org/10.1130/0016-7606(1979)90<1165:BSTHAP>2.0.CO;2)

1134 Elverhøi A, de Blasio F V, Butt FA, et al (2002) Submarine mass-wasting on glacially-
1135 influenced continental slopes: processes and dynamics. *Geol Soc London, Spec Publ*
1136 203:73–87. <https://doi.org/10.1144/GSL.SP.2002.203.01.05>

1137 Embley RW (1982) Anatomy of some Atlantic margin sediment slides and some comments
1138 on ages and mechanisms. In: *Marine Slides and Other Mass Movements*. Springer, pp
1139 189–213

1140 Enet F, Grilli ST (2007) Experimental study of tsunami generation by three-dimensional rigid
1141 underwater landslides. *J Waterw Port, Coastal, Ocean Eng* 133:442–454.
1142 [https://doi.org/10.1061/\(ASCE\)0733-950X\(2007\)133:6\(442\)](https://doi.org/10.1061/(ASCE)0733-950X(2007)133:6(442))

1143 Fernando HJS, McCulley JL, Mendis SG, Perera K (2005) Coral poaching worsens tsunami
1144 destruction in Sri Lanka. *Eos, Trans Am Geophys Union* 86:301–304.
1145 <https://doi.org/10.1029/2005EO330002>

1146 Ferrari R, Bryson M, Bridge T, et al (2016) Quantifying the response of structural complexity
1147 and community composition to environmental change in marine communities. *Glob*

1148 Chang Biol 22:1965–1975. <https://doi.org/10.1111/gcb.13197>

1149 Ferrario F, Beck MW, Storlazzi CD, et al (2014) The effectiveness of coral reefs for coastal
 1150 hazard risk reduction and adaptation. *Nat Commun* 5:3794.
 1151 <https://doi.org/10.1038/ncomms4794>

1152 Fine I V, Rabinovich AB, Bornhold BD, et al (2005) The Grand Banks landslide-generated
 1153 tsunami of November 18, 1929: preliminary analysis and numerical modeling. *Mar Geol*
 1154 215:45–57. <https://doi.org/10.1016/j.margeo.2004.11.007>

1155 Ford M, Becker JM, Merrifield MA, Song YT (2014) Marshall Islands Fringing Reef and
 1156 Atoll Lagoon Observations of the Tohoku Tsunami. *Pure Appl Geophys* 171:3351–
 1157 3363. <https://doi.org/10.1007/s00024-013-0757-8>

1158 Freire F, Gyllencreutz R, Jafri RU, Jakobsson M (2014) Acoustic evidence of a submarine
 1159 slide in the deepest part of the Arctic, the Molloy Hole. *Geo-Marine Lett* 34:315–325

1160 Frey-Martínez J, Cartwright J, James D (2006) Frontally confined versus frontally emergent
 1161 submarine landslides: a 3D seismic characterisation. *Mar Pet Geol* 23:585–604.
 1162 <https://doi.org/10.1016/j.marpetgeo.2006.04.002>

1163 Fritz HM, Borrero JC, Synolakis CE, et al (2011) Insights on the 2009 South Pacific tsunami
 1164 in Samoa and Tonga from field surveys and numerical simulations. *Earth-Science Rev*
 1165 107:66–75. <https://doi.org/10.1016/j.earscirev.2011.03.004>

1166 Fryer GJ, Watts P, Pratson LF (2004) Source of the great tsunami of 1 April 1946: a landslide
 1167 in the upper Aleutian forearc. *Mar Geol* 203:201–218. [https://doi.org/10.1016/S0025-3227\(03\)00305-0](https://doi.org/10.1016/S0025-3227(03)00305-0)

1169 Fujii Y, Satake K, Sakai S, et al (2011) Tsunami source of the 2011 off the Pacific coast of
 1170 Tohoku Earthquake. *Earth, Planets Sp* 63:55. <https://doi.org/10.5047/eps.2011.06.010>

1171 Gallop SL, Young IR, Ranasinghe R, et al (2014) The large-scale influence of the Great
 1172 Barrier Reef matrix on wave attenuation. *Coral Reefs* 33:1167–1178.
 1173 <https://doi.org/10.1007/s00338-014-1205-7>

1174 Gamberi F, Rovere M, Marani M (2011) Mass-transport complex evolution in a tectonically
 1175 active margin (Gioia Basin, Southeastern Tyrrhenian Sea). *Mar Geol* 279:98–110.
 1176 <https://doi.org/10.1016/j.margeo.2010.10.015>

1177 Gardner J V, Prior DB, Field ME (1999) Humboldt slide—a large shear-dominated
 1178 retrogressive slope failure. *Mar Geol* 154:323–338. [https://doi.org/10.1016/S0025-3227\(98\)00121-2](https://doi.org/10.1016/S0025-3227(98)00121-2)

1180 Garziglia S, Sultan N, Cattaneo A, et al (2010) Identification of Shear Zones and Their
 1181 Causal Mechanisms Using a Combination of Cone Penetration Tests and Seismic Data
 1182 in the Eastern Niger Delta. In: Mosher DC, Shipp RC, Moscardelli L, et al. (eds)
 1183 Submarine Mass Movements and Their Consequences. Springer Netherlands, Dordrecht,
 1184 pp 55–65

1185 Garziglia S, Sultan N, Cattaneo A, et al (2010) Identification of Shear Zones and Their
 1186 Causal Mechanisms Using a Combination of Cone Penetration Tests and Seismic Data
 1187 in the Eastern Niger Delta. In: Mosher DC, Shipp RC, Moscardelli L, et al. (eds)
 1188 Submarine Mass Movements and Their Consequences. Springer Netherlands, Dordrecht,
 1189 pp 55–65

1190 Gaullier V, Loncke L, Droz L, et al (2010) Slope instability on the French Guiana transform
 1191 margin from swath-bathymetry and 3.5 kHz echograms. In: Submarine Mass
 1192 Movements and Their Consequences. Springer, pp 569–579

1193 Gee MJR, Gawthorpe RL, Friedmann SJ (2006) Triggering and evolution of a giant
 1194 submarine landslide, offshore Angola, revealed by 3D seismic stratigraphy and
 1195 geomorphology. *J Sediment Res* 76:9–19. <https://doi.org/10.2110/jsr.2006.02>

1196 Gee MJR, Uy HS, Warren J, et al (2007) The Brunei slide: a giant submarine landslide on the
1197 North West Borneo Margin revealed by 3D seismic data. *Mar Geol* 246:9–23.
1198 <https://doi.org/10.1016/j.margeo.2007.07.009>

1199 Geersen J, Völker D, Behrmann JH, et al (2011) Pleistocene giant slope failures offshore
1200 Arauco peninsula, southern Chile. *J Geol Soc London* 168:1237–1248.
1201 <https://doi.org/10.1144/0016-76492011-027>

1202 Geist EL, Lynett PJ, Chaytor JD (2009) Hydrodynamic modeling of tsunamis from the
1203 Currituck landslide. *Mar Geol* 264:41–52. <https://doi.org/10.1016/j.margeo.2008.09.005>

1204 Gelfenbaum G, Apotsos A, Stevens AW, Jaffe B (2011) Effects of fringing reefs on tsunami
1205 inundation: American Samoa. *Earth-Science Rev* 107:12–22.
1206 <https://doi.org/10.1016/j.earscirev.2010.12.005>

1207 Georgiopoulou A, Masson DG, Wynn RB, Krastel S (2010) Sahara Slide: Age, initiation, and
1208 processes of a giant submarine slide. *Geochemistry, Geophys Geosystems* 11:
1209 <https://doi.org/10.1029/2010GC003066>

1210 Giles MK, Mosher DC, Piper DJW, Wach GD (2010) Mass transport deposits on the
1211 southwestern Newfoundland Slope. In: *Submarine Mass Movements and Their*
1212 *Consequences*. Springer, pp 657–665

1213 Glimsdal S, Pedersen GK, Harbitz CB, Løvholt F (2013) Dispersion of tsunamis: does it
1214 really matter? *Nat Hazards Earth Syst Sci* 13:1507–1526. [https://doi.org/10.5194/nhess-](https://doi.org/10.5194/nhess-13-1507-2013)
1215 [13-1507-2013](https://doi.org/10.5194/nhess-13-1507-2013)

1216 Goldfinger C, Kulm LD, McNeill LC, Watts P (2000) Super-scale failure of the southern
1217 Oregon Cascadia margin. *Pure Appl Geophys* 157:1189–1226.
1218 <https://doi.org/10.1007/s000240050023>

1219 Graham NAJ, Nash KL (2013) The importance of structural complexity in coral reef
1220 ecosystems. *Coral Reefs* 32:315–326. <https://doi.org/10.1007/s00338-012-0984-y>

1221 Grantz A, Phillips RL, Mullen MW, et al (1996) Character, paleoenvironment, rate of
1222 accumulation, and evidence for seismic triggering of Holocene turbidites, Canada
1223 Abyssal Plain, Arctic Ocean. *Mar Geol* 133:51–73. [https://doi.org/10.1016/0025-](https://doi.org/10.1016/0025-3227(96)00015-1)
1224 [3227\(96\)00015-1](https://doi.org/10.1016/0025-3227(96)00015-1)

1225 Greenslade DJM, Simanjuntak MA, Allen SCR (2009) An enhanced tsunami scenario
1226 database: T2. Center for Australian Weather and Climate Research (CAWCR) Technical
1227 Report No. 014

1228 Grilli ST, Harris JC, Shi F, et al (2012) Numerical modeling of coastal tsunami impact
1229 dissipation and impact. *Coast Eng Proc* 1:1–12

1230 Grilli ST, O'Reilly C, Harris JC, et al (2015) Modeling of SMF tsunami hazard along the
1231 upper US East Coast: detailed impact around Ocean City, MD. *Nat Hazards* 76:705–
1232 746. <https://doi.org/10.1007/s11069-014-1522-8>

1233 Grindlay N (1998) Volume and Density Approximations of Material Involved in a Debris
1234 Avalanche on the South Slope of the Puerto Rico Trench: A Report to the Puerto Rico
1235 Civil Defense and the University of Puerto Rico Sea Grant College Program. Univ
1236 North Carolina Wilmingt

1237 Haflidason H, Lien R, Sejrup HP, et al (2005) The dating and morphometry of the Storegga
1238 Slide. *Mar Pet Geol* 22:123–136. <https://doi.org/10.1016/j.marpetgeo.2004.10.008>

1239 Hampton MA, Lee HJ, Locat J (1996) Submarine landslides. *Rev Geophys* 34:33–59.
1240 <https://doi.org/10.1029/95RG03287>

1241 Harbitz CB, Løvholt F, Bungum H (2014) Submarine landslide tsunamis: How extreme and
1242 how likely? *Nat Hazards* 72:1341–1374. <https://doi.org/10.1007/s11069-013-0681-3>

1243 Harders R, Ranero CR, Weinrebe W, Behrmann JH (2011) Submarine slope failures along
1244 the convergent continental margin of the Middle America Trench. *Geochemistry,*
1245 *Geophys Geosystems* 12:n/a-n/a. <https://doi.org/10.1029/2010GC003401>

1246

1247 Harris DL, Rovere A, Casella E, et al (2018) Coral reef structural complexity provides
 1248 important coastal protection from waves under rising sea levels. *Sci Adv* 4:eao4350.
 1249 <https://doi.org/10.1126/sciadv.aao4350>

1250 Hengesh J V, Dirstein JK, Stanley AJ (2013) Landslide geomorphology along the Exmouth
 1251 plateau continental margin, North West Shelf, Australia. *Aust Geomech* 48:71–92

1252 Henrich R, Hanebuth TJJ, Krastel S, et al (2008) Architecture and sediment dynamics of the
 1253 Mauritania Slide Complex. *Mar Pet Geol* 25:17–33.
 1254 <https://doi.org/10.1016/j.marpetgeo.2007.05.008>

1255 Hieke W, Werner F (2000) The Augias megaturbidite in the central Ionian Sea (central
 1256 Mediterranean) and its relation to the Holocene Santorini event. *Sediment Geol*
 1257 135:205–218. [https://doi.org/10.1016/S0037-0738\(00\)00072-5](https://doi.org/10.1016/S0037-0738(00)00072-5)

1258 Hine AC, Locker SD, Tedesco LP, et al (1992) Megabreccia shedding from modern, low-
 1259 relief carbonate platforms, Nicaraguan Rise. *GSA Bull* 104:928–943.
 1260 [https://doi.org/10.1130/0016-7606\(1992\)104<0928:MSFMLR>2.3.CO;2](https://doi.org/10.1130/0016-7606(1992)104<0928:MSFMLR>2.3.CO;2)

1261 Hinstrosa G, Webster JM, Beaman RJ (2016) Postglacial sediment deposition along a mixed
 1262 carbonate-siliciclastic margin: New constraints from the drowned shelf-edge reefs of the
 1263 Great Barrier Reef, Australia. *Palaeogeogr Palaeoclimatol Palaeoecol* 446:168–185.
 1264 <https://doi.org/10.1016/j.palaeo.2016.01.023>

1265 Hjelstuen BO, Eldholm O, Faleide JJ (2007) Recurrent Pleistocene mega-failures on the SW
 1266 Barents Sea margin. *Earth Planet Sci Lett* 258:605–618.
 1267 <https://doi.org/10.1016/j.epsl.2007.04.025>

1268 Holcomb RT, Searle RC (1991) Large landslides from oceanic volcanoes. *Mar Georesources*
 1269 *Geotechnol* 10:19–32. <https://doi.org/10.1080/10641199109379880>

1270 Holmes R, Long D, Dodd LR (1998) Large-scale debrites and submarine landslides on the
 1271 Barra Fan, west of Britain. *Geol Soc London, Spec Publ* 129:67–79.
 1272 <https://doi.org/10.1144/GSL.SP.1998.129.01.05>

1273 Hopley D, Smithers SG, Parnell K (2007) The geomorphology of the Great Barrier Reef:
 1274 development, diversity and change. Cambridge University Press, Cambridge

1275 Horozal S, Bahk JJ, Lee SH, et al (2016) Late Neogene–Quaternary submarine mass wasting
 1276 along the margins of the Ulleung Basin, East Sea: Geomorphologic controls and
 1277 geohazard potential. *Quat Int* 392:69–98. <https://doi.org/10.1016/j.quaint.2015.06.056>

1278 Horrillo J, Wood A, Kim G, Parambath A (2013) A simplified 3-D Navier-Stokes numerical
 1279 model for landslide-tsunami: Application to the Gulf of Mexico. *J Geophys Res Ocean*
 1280 118:6934–6950. <https://doi.org/10.1002/2012JC008689>

1281 Hubble T, Webster J, Yu P, et al (2016) Submarine Landslides and Incised Canyons of the
 1282 Southeast Queensland Continental Margin. In: Lamarche G, Mountjoy J, Bull S, et al.
 1283 (eds) *Submarine Mass Movements and their Consequences: 7th International*
 1284 *Symposium*. Springer International Publishing, Cham, pp 125–134

1285 Hughes TP, Kerry JT, Baird AH, et al (2018) Global warming transforms coral reef
 1286 assemblages. *Nature* 556:492–496. <https://doi.org/10.1038/s41586-018-0041-2>

1287 Hühnerbach V, Masson DG, Bohrmann G, et al (2005) Deformation and submarine
 1288 landsliding caused by seamount subduction beneath the Costa Rica continental margin
 1289 — new insights from high-resolution sidescan sonar data. *Geol Soc London, Spec Publ*
 1290 244:195–205. <https://doi.org/10.1144/GSL.SP.2005.244.01.12>

1291 Hunt JE, Wynn RB, Talling PJ, Masson DG (2013) Frequency and timing of landslide-
 1292 triggered turbidity currents within the Agadir Basin, offshore NW Africa: Are there
 1293 associations with climate change, sea level change and slope sedimentation rates? *Mar*
 1294 *Geol* 346:274–291. <https://doi.org/10.1016/j.margeo.2013.09.004>

1295 Hunt JE (2012) Determining the provenance, recurrence, magnitudes and failure mechanisms
1296 of submarine landslides from the Moroccan margin and Canary Islands using distal
1297 turbidite records. University of Southampton

1298 Iacono C Lo, Gràcia E, Zaniboni F, et al (2012) Large, deepwater slope failures: implications
1299 for landslide-generated tsunamis. *Geology* 40:931–934.
1300 <https://doi.org/10.1130/G33446.1>

1301 Kazolea M, Filippini A, Ricchiuto M, et al (2019) Wave propagation, breaking, and
1302 overtopping on a 2D reef: A comparative evaluation of numerical codes for tsunami
1303 modelling. *Eur J Mech - B/Fluids* 73:122–131.
1304 <https://doi.org/10.1016/j.euromechflu.2017.10.010>

1305 Kim D-H, Lynett PJ, Socolofsky SA (2009) A depth-integrated model for weakly dispersive,
1306 turbulent, and rotational fluid flows. *Ocean Model* 27:198–214.
1307 <https://doi.org/10.1016/j.ocemod.2009.01.005>

1308 Koshimura S, Namegaya Y, Yanagisawa H (2009) Tsunami fragility: A new measure to
1309 identify tsunami damage. *J Disaster Res* 4:479–488.
1310 <https://doi.org/10.20965/jdr.2009.p0479>

1311 Kowalik Z, Knight W, Logan T, Whitmore P (2005) Numerical modeling of the global
1312 tsunami: Indonesian tsunami of 26 December 2004. *Sci Tsunami Hazards* 23:40–56

1313 Krastel S, Wynn RB, Georgiopoulou A, et al (2012) Large-Scale Mass Wasting on the
1314 Northwest African Continental Margin: Some General Implications for Mass Wasting
1315 on Passive Continental Margins. In: Yamada Y, Kawamura K, Ikehara K, et al. (eds)
1316 *Submarine Mass Movements and Their Consequences*. Springer Netherlands, Dordrecht,
1317 pp 189–199

1318 Kunkel CM, Hallberg RW, Oppenheimer M (2006) Coral reefs reduce tsunami impact in
1319 model simulations. *Geophys Res Lett* 33:L23612.
1320 <https://doi.org/10.1029/2006GL027892>

1321 Kvalstad TJ, Gauer P, Kayina AM, et al (2002) Slope stability at Ormen Lange: Offshore site
1322 investigation and geotechnics. In: *Diversity and Sustainability, Proceedings of an*
1323 *International Conference, London*. pp 233 –250

1324 Laberg JS, Kawamura K, Amundsen H, et al (2014) A submarine landslide complex affecting
1325 the Jan Mayen Ridge, Norwegian–Greenland Sea: slide-scar morphology and processes
1326 of sediment evacuation. *Geo-Marine Lett* 34:51–58

1327 Lallemand S, Lehu R, Rétif F, et al (2015) A ~3000 years-old sequence of extreme events
1328 revealed by marine and shore deposits east of Taiwan. *Tectonophysics* 692:325–341.
1329 <https://doi.org/10.1016/j.tecto.2015.11.001>

1330 Lamarche G, Joanne C, Collot J (2008) Successive, large mass-transport deposits in the south
1331 Kermadec fore-arc basin, New Zealand: The Matakaoa Submarine Instability Complex.
1332 *Geochemistry, Geophys Geosystems* 9:. <https://doi.org/10.1029/2007GC001843>

1333 Lastras G, Canals M, Urgeles R, et al (2007) A walk down the Cap de Creus canyon,
1334 Northwestern Mediterranean Sea: Recent processes inferred from morphology and
1335 sediment bedforms. *Mar Geol* 246:176–192.
1336 <https://doi.org/10.1016/j.margeo.2007.09.002>

1337 Lastras G, De Blasio FV, Canals M, Elverhøi A (2005) Conceptual and numerical modeling
1338 of the BIG'95 debris flow, western Mediterranean Sea. *J Sediment Res* 75:784–797.
1339 <https://doi.org/10.2110/jsr.2005.063>

1340 Le Friant A, Ishizuka O, Boudon G, et al (2015) Submarine record of volcanic island
1341 construction and collapse in the Lesser Antilles arc: First scientific drilling of submarine
1342 volcanic island landslides by IODPEXpedition 340. *Geochemistry, Geophys Geosystems*
1343 16:420–442. <https://doi.org/10.1002/2014GC005652>

- 1344 Lebas E, Le Friant A, Boudon G, et al (2011) Multiple widespread landslides during the
 1345 long-term evolution of a volcanic island: Insights from high-resolution seismic data,
 1346 Montserrat, Lesser Antilles. *Geochemistry, Geophys Geosystems* 12:Q05006.
 1347 <https://doi.org/10.1029/2010GC003451>
- 1348 Lebreiro SM, McCave IN, Weaver PPE (1997) Late Quaternary turbidite emplacement on the
 1349 Horseshoe abyssal plain (Iberian margin). *J Sediment Res Sect A Sediment Petrol*
 1350 *Process* 67:856–870
- 1351 Lee C, Nott JA, Keller FB, Parrish AR (2004) Seismic expression of the Cenozoic mass
 1352 transport complexes, deepwater Tarfaya-Agadir Basin, offshore Morocco. In: *Offshore*
 1353 *Technology Conference*. Offshore Technology Conference, Houston, Texas, p OTC-
 1354 16741-MS
- 1355 Lee HJ, Normark WR, Fisher MA, et al (2004) Timing and extent of submarine landslides in
 1356 Southern California. In: *Offshore Technology Conference*. Offshore Technology
 1357 *Conference*, Houston, Texas, p OTC-16744-MS
- 1358 Lee HJ (2009) Timing of occurrence of large submarine landslides on the Atlantic Ocean
 1359 margin. *Mar Geol* 264:53–64. <https://doi.org/10.1016/j.margeo.2008.09.009>
- 1360 Leslie SC, Mann P (2016) Giant submarine landslides on the Colombian margin and tsunami
 1361 risk in the Caribbean Sea. *Earth Planet Sci Lett* 449:382–394.
 1362 <https://doi.org/10.1016/j.epsl.2016.05.040>
- 1363 Li L, Switzer AD, Wang Y, et al (2015) What caused the mysterious eighteenth century
 1364 tsunami that struck the southwest Taiwan coast? *Geophys Res Lett* 42:8498–8506.
 1365 <https://doi.org/10.1002/2015GL065567>
- 1366 Li L, Switzer AD, Wang Y, et al (2018) A modest 0.5-m rise in sea level will double the
 1367 tsunami hazard in Macau. *Sci Adv* 4:eaat1180. <https://doi.org/10.1126/sciadv.aat1180>
- 1368 Lindberg B, Laberg JS, Vorren TO (2004) The Nyk Slide—morphology, progression, and
 1369 age of a partly buried submarine slide offshore northern Norway. *Mar Geol* 213:277–
 1370 289. <https://doi.org/10.1016/j.margeo.2004.10.010>
- 1371 Liu PLF, Lynett P, Fernando H, et al (2005) Observations by the International Tsunami
 1372 Survey Team in Sri Lanka. *Science* 308:1595. <https://doi.org/10.1126/science.1110730>
- 1373 Locat J, Brink US ten, Chaytor JD (2010) The Block Composite Submarine Landslide,
 1374 Southern New England Slope, U.S.A.: A Morphological Analysis. In: Mosher DC,
 1375 Shipp RC, Moscardelli L, et al. (eds) *Submarine Mass Movements and Their*
 1376 *Consequences*. Springer Netherlands, Dordrecht, pp 267–277
- 1377 Locat J, Lee H, Uri S, et al (2009) Geomorphology, stability and mobility of the Currituck
 1378 slide. *Mar Geol* 264:28–40. <https://doi.org/10.1016/j.margeo.2008.12.005>
- 1379 Longpré M-A, Chadwick JP, Wijbrans J, Iping R (2011) Age of the El Golfo debris
 1380 avalanche, El Hierro (Canary Islands): New constraints from laser and furnace
 1381 $^{40}\text{Ar}/^{39}\text{Ar}$ dating. *J Volcanol Geotherm Res* 203:76–80.
 1382 <https://doi.org/10.1016/j.jvolgeores.2011.04.002>
- 1383 Lowe RJ, Shavit U, Falter JL, et al (2008) Modeling flow in coral communities with and
 1384 without waves: A synthesis of porous media and canopy flow approaches. *Limnol*
 1385 *Oceanogr* 53:1595. <https://doi.org/10.4319/lo.2008.53.6.2668>
- 1386 Ma G, Kirby JT, Shi F (2013) Numerical simulation of tsunami waves generated by
 1387 deformable submarine landslides. *Ocean Model* 69:146–165.
 1388 <https://doi.org/10.1016/j.ocemod.2013.07.001>
- 1389 Madin JS, Connolly SR (2006) Ecological consequences of major hydrodynamic
 1390 disturbances on coral reefs. *Nature* 444:477–480. <https://doi.org/10.1038/nature05328>
- 1391 Maslin M, Vilela C, Mikkelsen N, Grootes P (2005) Causes of catastrophic sediment failures
 1392 of the Amazon Fan. *Quat Sci Rev* 24:2180–2193.
 1393 <https://doi.org/10.1016/j.quascirev.2005.01.016>

1394 Masson DG, Watts AB, Gee MJR, et al (2002) Slope failures on the flanks of the western
1395 Canary Islands. *Earth-Science Rev* 57:1–35. <https://doi.org/10.1016/S0012->
1396 8252(01)00069-1

1397 Masson DG, Harbitz CB, Wynn RB, et al (2006) Submarine landslides: processes, triggers
1398 and hazard prediction. *Philos Trans R Soc London A Math Phys Eng Sci* 364:2009–
1399 2039. <https://doi.org/10.1098/rsta.2006.1810>

1400 McAdoo BG, Ah-Leong JS, Bell L, et al (2011) Coral reefs as buffers during the 2009 South
1401 Pacific tsunami, Upolu Island, Samoa. *Earth-Science Rev* 107:147–155.
1402 <https://doi.org/10.1016/j.earscirev.2010.11.005>

1403 McAdoo BG, Moore A, Baumwoll J (2009) Indigenous knowledge and the near field
1404 population response during the 2007 Solomon Islands tsunami. *Nat Hazards* 48:73–82.
1405 <https://doi.org/10.1007/s11069-008-9249-z>

1406 McAdoo BG, Pratson LF, Orange DL (2000) Submarine landslide geomorphology, US
1407 continental slope. *Mar Geol* 169:103–136. <https://doi.org/10.1016/S0025->
1408 3227(00)00050-5

1409 McGregor BA, Rothwell RG, Kenyon NH, Twichell DC (1993) Salt tectonics and slope
1410 failure in an area of salt domes in the northwestern Gulf of Mexico. In: *Submarine*
1411 *landslides: selected studies in the US Exclusive Economic Zone*. US Geological Survey
1412 *Bulletin*, pp 92–96

1413 McMurtry GM, Watts P, Fryer GJ, et al (2004) Giant landslides, mega-tsunamis, and paleo-
1414 sea level in the Hawaiian Islands. *Mar Geol* 203:219–233.
1415 [https://doi.org/10.1016/S0025-3227\(03\)00306-2](https://doi.org/10.1016/S0025-3227(03)00306-2)

1416 Meyer M, Geersen J, Krastel S, et al (2012) Dakar Slide Offshore Senegal, NW-Africa:
1417 Interaction of Stacked Giant Mass Wasting Events and Canyon Evolution. In: Yamada
1418 Y, Kawamura K, Ikehara K, et al. (eds) *Submarine Mass Movements and Their*
1419 *Consequences*. Springer Netherlands, Dordrecht, pp 177–188

1420 Monismith SG, Herdman LMM, Ahmerkamp S, Hench JL (2013) Wave transformation and
1421 wave-driven flow across a steep coral reef. *J Phys Oceanogr* 43:1356–1379.
1422 <https://doi.org/10.1175/JPO-D-12-0164.1>

1423 Moore DG, Curray JR, Emmel FJ (1976) Large submarine slide (olistostrome) associated
1424 with Sunda Arc subduction zone, northeast Indian Ocean. *Mar Geol* 21:211–226.
1425 [https://doi.org/10.1016/0025-3227\(76\)90060-8](https://doi.org/10.1016/0025-3227(76)90060-8)

1426 Moore GF, Strasser M (2016) Large Mass Transport Deposits in Kumano Basin, Nankai
1427 Trough, Japan. In: Lamarche G, Mountjoy J, Bull S, et al. (eds) *Submarine Mass*
1428 *Movements and their Consequences: 7th International Symposium*. Springer
1429 International Publishing, Cham, pp 371–379

1430 Moore JG, Clague DA, Holcomb RT, et al (1989) Prodigious submarine landslides on the
1431 Hawaiian Ridge. *J Geophys Res Solid Earth* 94:17465–17484.
1432 <https://doi.org/10.1029/JB094iB12p17465>

1433 Moore JG, Clague DA (2002) Mapping the Nuuanu and Wailau landslides in Hawaii.
1434 *Hawaiian Volcanoes Deep Underw Perspect* 128:223–244.
1435 <https://doi.org/10.1029/GM128p0223>

1436 Mori N, Takahashi T, Yasuda T, Yanagisawa H (2011) Survey of 2011 Tohoku earthquake
1437 tsunami inundation and run-up. *Geophys Res Lett* 38:6–11.
1438 <https://doi.org/10.1029/2011GL049210>

1439 Moscardelli L, Wood L (2008) New classification system for mass transport complexes in
1440 offshore Trinidad. *Basin Res* 20:73–98. <https://doi.org/10.1111/j.1365->
1441 2117.2007.00340.x

1442 Moscardelli L, Wood L, Mann P (2006) Mass-transport complexes and associated processes
1443 in the offshore area of Trinidad and Venezuela. *Am Assoc Pet Geol Bull* 90:1059–1088.
1444 <https://doi.org/10.1306/02210605052>

1445 Moscardelli L, Wood L (2016) Morphometry of mass-transport deposits as a predictive tool.
1446 *Bull Geol Soc Am* 128:47–80. <https://doi.org/10.1130/B31221.1>

1447 Mosher DC, Xu Z, Shimeld J (2010) The Pliocene Shelburne Mass-Movement and
1448 Consequent Tsunami, Western Scotian Slope BT - Submarine Mass Movements and
1449 Their Consequences. In: Mosher DC, Shipp RC, Moscardelli L, et al. (eds). Springer
1450 Netherlands, Dordrecht, pp 765–775

1451 Mountjoy JJ, McKean J, Barnes PM, Pettinga JR (2009) Terrestrial-style slow-moving
1452 earthflow kinematics in a submarine landslide complex. *Mar Geol* 267:114–127.
1453 <https://doi.org/10.1016/j.margeo.2009.09.007>

1454 Mountjoy JJ, Micallef A (2012) Polyphase Emplacement of a 30 km³ Blocky Debris
1455 Avalanche and Its Role in Slope-Gully Development. In: Yamada Y, Kawamura K,
1456 Ikehara K, et al. (eds) *Submarine Mass Movements and Their Consequences*. Springer
1457 Netherlands, Dordrecht, pp 213–222

1458 Mullins HT, Dolan J, Breen N, et al (1991) Retreat of carbonate platforms: response to
1459 tectonic processes. *Geology* 19:1089–1092. [https://doi.org/10.1130/0091-](https://doi.org/10.1130/0091-7613(1991)019<1089:ROCPRT>2.3.CO;2)
1460 [7613\(1991\)019<1089:ROCPRT>2.3.CO;2](https://doi.org/10.1130/0091-7613(1991)019<1089:ROCPRT>2.3.CO;2)

1461 Nagai R, Takabatake T, Esteban M, et al (2020) Tsunami risk hazard in Tokyo Bay: The
1462 challenge of future sea level rise. *Int J Disaster Risk Reduct* 45:101321.
1463 <https://doi.org/https://doi.org/10.1016/j.ijdr.2019.101321>

1464 National Geophysical Data Center / World Data Service (2020) Global Historical Tsunami
1465 Database. NOAA National Centers for Environmental Information

1466 National Tsunami Hazard Mitigation Program (NTHMP) (2012) Proceedings and results of
1467 the 2011 NTHMP model benchmarking workshop. US Dept. of Commerce, NOAA, and
1468 NTHMP Boulder, CO

1469 Nelson RC (1996) Hydraulic roughness of coral reef platforms. *Appl Ocean Res* 18:265–274.
1470 [https://doi.org/10.1016/S0141-1187\(97\)00006-0](https://doi.org/10.1016/S0141-1187(97)00006-0)

1471 Newton CS, Shipp RC, Mosher DC, Wach GD (2004) Importance of mass transport
1472 complexes in the Quaternary development of the Nile Fan, Egypt. In: *Offshore*
1473 *Technology Conference*. Offshore Technology Conference, Houston, Texas

1474 Nielsen P (1992) Coastal Bottom Boundary Layers and Sediment Transport. World
1475 Scientific, Singapore

1476 Niemi TM, Ben-Avraham Z, Hartnady CJH, Reznikov M (2000) Post-Eocene seismic
1477 stratigraphy of the deep ocean basin adjacent to the southeast African continental
1478 margin: a record of geostrophic bottom current systems. *Mar Geol* 162:237–258.
1479 [https://doi.org/10.1016/S0025-3227\(99\)00062-6](https://doi.org/10.1016/S0025-3227(99)00062-6)

1480 Nistor I, Palermo D, Nouri Y, et al (2009) Tsunami-Induced Forces on Structures. In: Kim
1481 YC (ed) *Handbook of Coastal and Ocean Engineering*. World Scientific, pp 261–286

1482 Normark WR, Gutmacher CE (1988) Sur submarine slide, Monterey fan, central California.
1483 *Sedimentology* 35:629–647. <https://doi.org/10.1111/j.1365-3091.1988.tb01241.x>

1484 Nott J (1997) Extremely high-energy wave deposits inside the Great Barrier Reef, Australia:
1485 Determining the cause-tsunami or tropical cyclone. *Mar Geol* 141:193–207.
1486 [https://doi.org/10.1016/S0025-3227\(97\)00063-7](https://doi.org/10.1016/S0025-3227(97)00063-7)

1487 Nouri Y, Nistor I, Palermo DAN, Cornett A (2010) Experimental investigation of tsunami
1488 impact on free standing structures. *Coast Eng J* 52:43–70.
1489 <https://doi.org/10.1142/S0578563410002117>

1490 Nygård A, Sejrup HP, Haflidason H, Bryn P (2005) The glacial North Sea Fan, southern
1491 Norwegian Margin: architecture and evolution from the upper continental slope to the

1492 deep-sea basin. *Mar Pet Geol* 22:71–84.
1493 <https://doi.org/10.1016/j.marpetgeo.2004.12.001>
1494 Okada Y (1985) Surface deformation due to shear and tensile faults in a half-space. *Bull*
1495 *Seismol Soc Am* 75:1135–1154
1496 Omira R, Ramalho I, Terrinha P, et al (2016) Deep-water seamounts, a potential source of
1497 tsunami generated by landslides? The Hironnelle Seamount, NE Atlantic. *Mar Geol*
1498 379:267–280. <https://doi.org/10.1016/j.margeo.2016.06.010>
1499 Omosanya KO, Alves TM (2013) A 3-dimensional seismic method to assess the provenance
1500 of mass-transport deposits (MTDs) on salt-rich continental slopes (Espírito Santo Basin,
1501 SE Brazil). *Mar Pet Geol* 44:223–239. <https://doi.org/10.1016/j.marpetgeo.2013.02.006>
1502 Owen M, Day S, Long D, Maslin M (2010) Investigations on the Peach 4 Debrite, a Late
1503 Pleistocene Mass Movement on the Northwest British Continental Margin. In: Mosher
1504 DC, Shipp RC, Moscardelli L, et al. (eds) *Submarine Mass Movements and Their*
1505 *Consequences*. Springer Netherlands, Dordrecht, pp 301–311
1506 Owen M, Day S, Maslin M (2007) Late Pleistocene submarine mass movements: occurrence
1507 and causes. *Quat Sci Rev* 26:958–978. <https://doi.org/10.1016/j.quascirev.2006.12.011>
1508 Papadopoulos GA, Gràcia E, Urgeles R, et al (2014) Historical and pre-historical tsunamis in
1509 the Mediterranean and its connected seas: Geological signatures, generation mechanisms
1510 and coastal impacts. *Mar Geol* 354:81–109.
1511 <https://doi.org/10.1016/j.margeo.2014.04.014>
1512 Piper DJW, Pirmez C, Manley PL, et al (1997) Mass-transport deposits of the Amazon Fan.
1513 In: *Proceedings of the Ocean Drilling Program, Scientific Results*. Ocean Drilling
1514 Program, College Station, Texas, pp 109–146
1515 Piper DJW, Aksu AE (1987) The source and origin of the 1929 grand banks turbidity current
1516 inferred from sediment budgets. *Geo-Marine Lett* 7:177–182.
1517 <https://doi.org/10.1007/BF02242769>
1518 Power HE, Clarke SL, Wilson O, Hubble TTCT (2015) Tsunami hazard from submarine
1519 landslides: 3D inundation modelling in New South Wales, Australia. In: *Australasian*
1520 *Coasts & Ports Conference 2015: 22nd Australasian Coastal and Ocean Engineering*
1521 *Conference and the 15th Australasian Port and Harbour Conference*. Engineers Australia
1522 and IPENZ, p 696
1523 Puga-Bernabéu Á, Beaman RJ, Webster JM, et al (2016) Gloria Knolls Slide: A prominent
1524 submarine landslide complex on the Great Barrier Reef margin of north-eastern
1525 Australia. *Mar Geol* 385:68–83. <https://doi.org/10.1016/j.margeo.2016.12.008>
1526 Puga-Bernabéu Á, Webster JM, Beaman RJ (2013a) Potential collapse of the upper slope and
1527 tsunami generation on the Great Barrier Reef margin, north-eastern Australia. *Nat*
1528 *Hazards* 66:557–575. <https://doi.org/10.1007/s11069-012-0502-0>
1529 Puga-Bernabéu Á, Webster JM, Beaman RJ, et al (2019) Submarine Landslides Along the
1530 Mixed Siliciclastic-Carbonate Margin of the Great Barrier Reef (Offshore Australia). In:
1531 *Submarine Landslides*. American Geophysical Union, pp 313–337
1532 Puga-Bernabéu Á, Webster JM, Beaman RJ, Guilbaud V (2011) Morphology and controls on
1533 the evolution of a mixed carbonate–siliciclastic submarine canyon system, Great Barrier
1534 Reef margin, north-eastern Australia. *Mar Geol* 289:100–116.
1535 <https://doi.org/10.1016/j.margeo.2011.09.013>
1536 Puga-Bernabéu Á, Webster JM, Beaman RJ, Guilbaud V (2013b) Variation in canyon
1537 morphology on the Great Barrier Reef margin, north-eastern Australia: The influence of
1538 slope and barrier reefs. *Geomorphology* 191:35–50.
1539 <https://doi.org/10.1016/j.geomorph.2013.03.001>
1540 Quataert E, Storlazzi C, van Rooijen A, et al (2015) The influence of coral reefs and climate
1541 change on wave-driven flooding of tropical coastlines. *Geophys Res Lett* 42:6407–6415.

1542 <https://doi.org/10.1002/2015GL064861>

1543 Ratzov G, Collot J-Y, Sosson M, Migeon S (2010) Mass-transport deposits in the northern
1544 Ecuador subduction trench: Result of frontal erosion over multiple seismic cycles. *Earth*
1545 *Planet Sci Lett* 296:89–102. <https://doi.org/10.1016/j.epsl.2010.04.048>

1546 Reeder MS, Stow DA V, Rothwell RG (2002) Late Quaternary turbidite input into the east
1547 Mediterranean basin: new radiocarbon constraints on climate and sea-level control. *Geol*
1548 *Soc London, Spec Publ* 191:267–278

1549 Rodriguez M, Chamot-Rooke N, Hébert H, et al (2013) Owen Ridge deep-water submarine
1550 landslides: implications for tsunami hazard along the Oman coast. *Nat Hazards Earth*
1551 *Syst Sci* 13:417–424. <https://doi.org/10.5194/nhess-13-417-2013>

1552 Rodriguez NM, Paull CK (2000) 32. DATA REPORT: 14C dating of sediment of the
1553 uppermost Cape Fear slide plain: constraints on the timing of this massive submarine
1554 landslide. *Proc Ocean Drill Program, Sci Results* 164:325–332

1555 Roeber V, Yamazaki Y, Cheung KF (2010) Resonance and impact of the 2009 Samoa
1556 tsunami around Tutuila, American Samoa. *Geophys Res Lett* 37:1–8.
1557 <https://doi.org/10.1029/2010GL044419>

1558 Roger J, Dudon B, Krien Y, Zahibo N (2014) Discussion about tsunami interaction with
1559 fringing coral reef. In: *Tsunami Events and Lessons Learned*. Springer, pp 161–176

1560 Rogers JS, Monismith SG, Kowek DA, Dunbar RB (2016) Wave dynamics of a Pacific
1561 Atoll with high frictional effects. *J Geophys Res Ocean* 121:350–367.
1562 <https://doi.org/10.1002/2015JC011170>

1563 Rosman JH, Hench JL (2011) A framework for understanding drag parameterizations for
1564 coral reefs. *J Geophys Res Ocean* 116:C08025. <https://doi.org/10.1029/2010JC006892>

1565 Rothwell RG, Thomson J, Kahler G (1998) Low-sea-level emplacement of a very large Late
1566 Pleistocene “megaturbidite” in the western Mediterranean Sea. *Nature* 392:377–380.
1567 <https://doi.org/10.1038/32871>

1568 San Pedro L, Babonneau N, Gutscher M-A, Cattaneo A (2016) Origin and chronology of the
1569 Augias deposit in the Ionian Sea (Central Mediterranean Sea), based on new regional
1570 sedimentological data. *Mar Geol* 384:199–213.
1571 <https://doi.org/10.1016/j.margeo.2016.05.005>

1572 Satake K (2007) Volcanic origin of the 1741 Oshima-Oshima tsunami in the Japan Sea.
1573 *Earth, Planets Sp* 59:381–390. <https://doi.org/10.1186/BF03352698>

1574 Satake K, Smith JR, Shinozaki K (2002) Three-Dimensional Reconstruction and Tsunami
1575 Model of the Nuuanu and Wailau Giant Landslides, Hawaii. In: *Hawaiian Volcanoes:*
1576 *Deep Underwater Perspectives*. Washington DC American Geophysical Union
1577 *Geophysical Monograph Series*, pp 333–346

1578 Sayago-Gil M, Long D, Hitchen K, et al (2010) Evidence for current-controlled morphology
1579 along the western slope of Hatton Bank (Rockall Plateau, NE Atlantic Ocean). *Geo-*
1580 *Marine Lett* 30:99–111. <https://doi.org/10.1007/s00367-009-0163-5>

1581 Schambach L, Grilli ST, Kirby JT, Shi F (2018) Landslide Tsunami Hazard Along the Upper
1582 US East Coast: Effects of Slide Deformation, Bottom Friction, and Frequency
1583 Dispersion. *Pure Appl Geophys* 176:1–40. <https://doi.org/10.1007/s00024-018-1978-7>

1584 Schnyder JSD, Eberli GP, Kirby JT, et al (2016) Tsunamis caused by submarine slope
1585 failures along western Great Bahama Bank. *Sci Rep* 6:1–9.
1586 <https://doi.org/10.1038/srep35925>

1587 Schwab JM, Krastel S, Grün M, et al (2012) Submarine mass wasting and associated tsunami
1588 risk offshore western Thailand, Andaman Sea, Indian Ocean. *Nat Hazards Earth Syst Sci*
1589 12:2609. <https://doi.org/10.5194/nhess-12-2609-2012>

- 1590 Schwab WC, Danforth WW, Scanlon KM, Masson DG (1991) A giant submarine slope
1591 failure on the northern insular slope of Puerto Rico. *Mar Geol* 96:237–246.
1592 [https://doi.org/10.1016/0025-3227\(91\)90149-X](https://doi.org/10.1016/0025-3227(91)90149-X)
- 1593 Shao K, Liu W, Gao Y, Ning Y (2019) The influence of climate change on tsunami-like
1594 solitary wave inundation over fringing reefs. *J Integr Environ Sci* 16:71–88.
1595 <https://doi.org/10.1080/1943815X.2019.1614071>
- 1596 Sheppard C, Dixon DJ, Gourlay M, et al (2005) Coral mortality increases wave energy
1597 reaching shores protected by reef flats: Examples from the Seychelles. *Estuar Coast*
1598 *Shelf Sci* 64:223–234. <https://doi.org/10.1016/j.ecss.2005.02.016>
- 1599 Shi F, Kirby JT, Harris JC, et al (2012) A high-order adaptive time-stepping TVD solver for
1600 Boussinesq modeling of breaking waves and coastal inundation. *Ocean Model* 43–
1601 44:36–51. <https://doi.org/10.1016/j.ocemod.2011.12.004>
- 1602 Shi F, Kirby JT, Tehranirad B, et al (2016) FUNWAVE-TVD fully nonlinear Boussinesq
1603 wave model with TVD solver - documentation and user's manual (Version 3.0). Center
1604 for Applied Coastal Research, University of Delaware. Report No.: CACR-11-03
- 1605 Smith BM, Deptuck ME, Kendell KL (2010) Upper Cretaceous mass transport systems above
1606 the Wyandot Formation chalk, offshore Nova Scotia. In: Mosher DC, Shipp C,
1607 Moscardelli L, et al. (eds) *Submarine Mass Movements and Their Consequences*,
1608 *Advances in Natural and Technological Hazards Research*, Kluger-Springer Book
1609 Series. Springer, pp 605–616
- 1610 Solheim A, Berg K, Forsberg CF, Bryn P (2005) The Storegga Slide complex: repetitive
1611 large scale sliding with similar cause and development. *Mar Pet Geol* 22:97–107.
1612 <https://doi.org/10.1016/j.marpetgeo.2004.10.013>
- 1613 Spalding MD, Brown BE (2015) Warm-water coral reefs and climate change. *Science*
1614 350:769 LP – 771. <https://doi.org/10.1126/science.aad0349>
- 1615 Spalding MD, Ruffo S, Lacambra C, et al (2014) The role of ecosystems in coastal
1616 protection: Adapting to climate change and coastal hazards. *Ocean Coast Manag* 90:50–
1617 57. <https://doi.org/10.1016/j.ocecoaman.2013.09.007>
- 1618 Storlazzi CD, Gingerich SB, van Dongeren A, et al (2018) Most atolls will be uninhabitable
1619 by the mid-21st century because of sea-level rise exacerbating wave-driven flooding. *Sci*
1620 *Adv* 4:eaap9741. <https://doi.org/10.1126/sciadv.aap9741>
- 1621 Synolakis CE, Bardet J-P, Borrero JC, et al (2002) The slump origin of the 1998 Papua New
1622 Guinea Tsunami. *Proc R Soc A Math Phys Eng Sci* 458:763–789.
1623 <https://doi.org/10.1098/rspa.2001.0915>
- 1624 Talukder AR, Völker D (2014) The Tsunami Generation Potential of Shovel and Bulli Slides
1625 in the Continental Margin SE Australia BT - *Submarine Mass Movements and Their*
1626 *Consequences: 6th International Symposium*. In: Krastel S, Behrmann J-H, Völker D, et
1627 al. (eds). Springer International Publishing, Cham, pp 539–548
- 1628 Tappin DR, Watts P, Grilli ST (2008) The Papua New Guinea tsunami of 17 July 1998:
1629 anatomy of a catastrophic event. *Nat Hazards Earth Syst Sci* 8:243–266
- 1630 Tappin DR, Grilli ST, Harris JC, et al (2014) Did a submarine landslide contribute to the
1631 2011 Tohoku tsunami? *Mar Geol* 357:344–361.
1632 <https://doi.org/10.1016/j.margeo.2014.09.043>
- 1633 Tappin DR, Matsumoto T, Watts P, et al (1999) Sediment slump likely caused 1998 Papua
1634 New Guinea tsunami. *Eos Trans Am Geophys Union* 80:329–340.
1635 <https://doi.org/10.1029/99EO00241>
- 1636 Tehranirad B, Harris JC, Grilli AR, et al (2015) Far-field tsunami impact in the North
1637 Atlantic basin from large scale flank collapses of the Cumbre Vieja Volcano, La Palma.
1638 *Pure Appl Geophys* 172:3589–3616
- 1639 Tehranirad B, Kirby JT, Ma G, Shi F (2012) Tsunami benchmark results for nonhydrostatic

1640 wave model NHWAVE (Version 1.1). Research Report No. CACR-11-02. Newark
1641 Ten Brink US, Geist EL, Andrews BD (2006) Size distribution of submarine landslides and
1642 its implication to tsunami hazard in Puerto Rico. *Geophys Res Lett* 33:L11307.
1643 <https://doi.org/10.1029/2006GL026125>
1644 Torelli L, Sartori R, Zitellini N (1997) The giant chaotic body in the Atlantic Ocean off
1645 Gibraltar: new results from a deep seismic reflection survey. *Mar Pet Geol* 14:125–134.
1646 [https://doi.org/10.1016/S0264-8172\(96\)00060-8](https://doi.org/10.1016/S0264-8172(96)00060-8)
1647 Urgeles R, Lastras G, Canals M, et al (2003) The Big '95 Debris Flow and Adjacent Unfailed
1648 Sediments in the NW Mediterranean Sea: Geotechnical sedimentological Properties, and
1649 Dating. In: Locat J, Mienert J, Boisvert L (eds) *Submarine Mass Movements and Their
1650 Consequences: 1st International Symposium*. Springer Netherlands, Dordrecht, pp 479–
1651 487
1652 Urgeles R, Leynaud D, Lastras G, et al (2006) Back-analysis and failure mechanisms of a
1653 large submarine slide on the Ebro slope, NW Mediterranean. *Mar Geol* 226:185–206.
1654 <https://doi.org/10.1016/j.margeo.2005.10.004>
1655 Urlaub M, Talling PJ, Masson DG (2013) Timing and frequency of large submarine
1656 landslides: Implications for understanding triggers and future geohazard. *Quat Sci Rev*
1657 72:63–82. <https://doi.org/10.1016/j.quascirev.2013.04.020>
1658 Uslu B, Titov V V., Eble M, Chamberlin CD (2010) Tsunami hazard assessment for Guam.
1659 NOAA Pacific Marine Environmental Laboratory Special Rep., National Oceanic and
1660 Atmospheric Administration, Seattle, WA, USA
1661 Van Weering TCE, Nielsen T, Kenyon NH, et al (1998) Sediments and sedimentation at the
1662 NE Faeroe continental margin; contourites and large-scale sliding. *Mar Geol* 152:159–
1663 176. [https://doi.org/10.1016/S0025-3227\(98\)00069-3](https://doi.org/10.1016/S0025-3227(98)00069-3)
1664 Vizcaino A, Gràcia E, Pallàs R, et al (2006) Sedimentology, physical properties and age of
1665 mass transport deposits associated with the Marques de Pombal Fault, Southwest
1666 Portuguese Margin. *Nor Geol Tidsskr* 86:177
1667 Voight B, Le Friant A, Boudon G, et al (2012) Undrained Sediment Loading Key to Long-
1668 Runout Submarine Mass Movements: Evidence from the Caribbean Volcanic Arc. In:
1669 Yamada Y, Kawamura K, Ikehara K, et al. (eds) *Submarine Mass Movements and Their
1670 Consequences*. Springer Netherlands, Dordrecht, pp 417–428
1671 Völker D, Geersen J, Behrmann JH, Weinrebe WR (2012) Submarine Mass Wasting Off
1672 Southern Central Chile: Distribution and Possible Mechanisms of Slope Failure at an
1673 Active Continental Margin. In: Yamada Y, Kawamura K, Ikehara K, et al. (eds)
1674 *Submarine Mass Movements and Their Consequences: 5th International Symposium*.
1675 Springer Netherlands, Dordrecht, pp 379–389
1676 von Huene R, Ranero CR, Weinrebe W, Hinz K (2000) Quaternary convergent margin
1677 tectonics of Costa Rica, segmentation of the Cocos Plate, and Central American
1678 volcanism. *Tectonics* 19:314–334. <https://doi.org/10.1029/1999TC001143>
1679 von Huene R, Bourgeois J, Miller J, Pautot G (1989) A large tsunamogenic landslide and
1680 debris flow along the Peru Trench. *J Geophys Res Solid Earth* 94:1703–1714.
1681 <https://doi.org/10.1029/JB094iB02p01703>
1682 Vorren TO, Laberg JS, Blaume F, et al (1998) The Norwegian–Greenland Sea continental
1683 margins: morphology and late Quaternary sedimentary processes and environment. *Quat
1684 Sci Rev* 17:273–302. [https://doi.org/10.1016/S0277-3791\(97\)00072-3](https://doi.org/10.1016/S0277-3791(97)00072-3)
1685 Wang X, Mountjoy J, Power WL, et al (2016) Coupled Modelling of the Failure and Tsunami
1686 of a Submarine Debris Avalanche Offshore Central New Zealand. In: Lamarche G,
1687 Mountjoy J, Bull S, et al. (eds) *Submarine Mass Movements and their Consequences:
1688 7th International Symposium*. Springer International Publishing, Cham, pp 599–606

- 1689 Ward SN, Day S (2003) Ritter Island volcano—lateral collapse and the tsunami of 1888.
 1690 *Geophys J Int* 154:891–902. <https://doi.org/10.1046/j.1365-246X.2003.02016.x>
- 1691 Ward SN, Asphaug E (2003) Asteroid impact tsunami of 2880 March 16. *Geophys J Int*
 1692 153:F6–F10. <https://doi.org/10.1046/j.1365-246X.2003.01944.x>
- 1693 Watts P, Grilli ST, Kirby JT, et al (2003) Landslide tsunami case studies using a Boussinesq
 1694 model and a fully nonlinear tsunami generation model. *Nat Hazards Earth Syst Sci*
 1695 3:391–402. <https://doi.org/10.5194/nhess-3-391-2003>
- 1696 Weaver PPE, Rothwell RG (1987) Sedimentation on the Madeira Abyssal Plain over the last
 1697 300 000 years. *Geol Soc London, Spec Publ* 31:71–86
- 1698 Webster JM, Davies PJ, Beaman RJ, et al (2008) Evolution of drowned shelf edge reefs in the
 1699 GBR; implications for understanding abrupt climate change, coral reef response and
 1700 modern deep water benthic habitats—RV Southern Surveyor—voyage summary.
 1701 Marine National Facility, Hobart, Tasmania, p 18
- 1702 Webster JM, George NPJ, Beaman RJ, et al (2016) Submarine landslides on the Great Barrier
 1703 Reef shelf edge and upper slope: A mechanism for generating tsunamis on the north-east
 1704 Australian coast? *Mar Geol* 371:120–129. <https://doi.org/10.1016/j.margeo.2015.11.008>
- 1705 Wei Y, Fritz HM, Titov V V., et al (2015) Source Models and Near-Field Impact of the 1
 1706 April 2007 Solomon Islands Tsunami. *Pure Appl Geophys* 172:657–682.
 1707 <https://doi.org/10.1007/s00024-014-1013-6>
- 1708 Wien K, Kölling M, Schulz HD (2007) Age models for the Cape Blanc Debris Flow and the
 1709 Mauritania Slide Complex in the Atlantic Ocean off NW Africa. *Quat Sci Rev* 26:2558–
 1710 2573. <https://doi.org/10.1016/j.quascirev.2007.06.018>
- 1711 Wild C, Hoegh-Guldberg O, Naumann MS, et al (2011) Climate change impedes
 1712 scleractinian corals as primary reef ecosystem engineers. *Mar Freshw Res* 62:205–215.
 1713 <https://doi.org/10.1071/MF10254>
- 1714 Williams SP, Davies TR, Barrows TT, et al (2014) Flank-Collapse on Ta’u Island, Samoan
 1715 Archipelago: Timing and Hazard Implications. In: Sassa K, Canuti P, Yin Y (eds)
 1716 *Landslide Science for a Safer Geoenvironment*. Springer International Publishing,
 1717 Cham, pp 583–588
- 1718 Winkelmann D, Geissler W, Schneider J, Stein R (2008) Dynamics and timing of the
 1719 Hinlopen/Yermak Megaslide north of Spitsbergen, Arctic Ocean. *Mar Geol* 250:34–50.
 1720 <https://doi.org/10.1016/j.margeo.2007.11.013>
- 1721 Wynn RB, Talling PJ, Masson DG, et al (2010) Investigating the Timing, Processes and
 1722 Deposits of One of the World’s Largest Submarine Gravity Flows: The ‘Bed 5 Event’
 1723 Off Northwest Africa. In: Mosher DC, Shipp RC, Moscardelli L, et al. (eds) *Submarine*
 1724 *Mass Movements and Their Consequences*. Springer Netherlands, Dordrecht, pp 463–
 1725 474
- 1726 Wynn RB, Masson DG, Stow DA, Weaver PP (2000) The Northwest African slope apron: a
 1727 modern analogue for deep-water systems with complex seafloor topography. *Mar Pet*
 1728 *Geol* 17:253–265. [https://doi.org/10.1016/S0264-8172\(99\)00014-8](https://doi.org/10.1016/S0264-8172(99)00014-8)
- 1729 Xing HL, Ding RW, Yuen D (2015) Tsunami Hazards along the Eastern Australian Coast
 1730 from Potential Earthquakes: Results from Numerical Simulations. *Pure Appl Geophys*
 1731 172:2087–2115. <https://doi.org/10.1007/s00024-014-0904-x>
- 1732 Yao Y, Huang Z, Monismith SG, Lo EYM (2012) 1DH Boussinesq modeling of wave
 1733 transformation over fringing reefs. *Ocean Eng* 47:30–42.
 1734 <https://doi.org/10.1016/j.oceaneng.2012.03.010>
- 1735 Yongfu S, Bolin H (2014) A potential tsunami impact assessment of submarine landslide at
 1736 Baiyun Depression in Northern South China Sea. *Geoenvironmental Disasters* 1:7.
 1737 <https://doi.org/10.1186/s40677-014-0007-0>
- 1738 Young IR (1989) Wave transformation over coral reefs. *J Geophys Res Ocean* 94:9779–

1739 9789. <https://doi.org/10.1029/JC094iC07p09779>
1740 Young IR, Hardy TA (1993) Measurement and modelling of tropical cyclone waves in the
1741 Great Barrier Reef. *Coral Reefs* 12:85–95. <https://doi.org/10.1007/BF00302108>
1742

Draft manuscript